Politecnico di Milano

ENERGY DEPARTMENT
DOCTORAL PROGRAMME IN ELECTRICAL ENGINEERING

SIGNAL PROCESSING FOR DISRUPTION DETECTION IN TOKAMAKS

Supervised by:
Prof. Gabriele D'ANTONA
Dr. Carlo SOZZI

Doctoral Dissertation of:
Maia MOSCONI
matr. 769131

Coordinator:
Prof. Alberto BERIZZI

Year 2013-2014 Cycle XXVI

Contents

List of Figures

List of Tables

Abstract

Disruptions in tokamaks occur as sudden fall of plasma current and lost of magnetic confinement with dangerous consequences on the integrity of the machine. In order to obtain a sufficient gain from thermonuclear fusion reactions, it is necessary to operate in conditions of high current, pressure and density. In this regime disruptions can occur and pose a danger for the device. It is important to classify the causes of disruption and develop strategy for disruption avoidance and or/mitigation.
This PhD project concerns the identification of a precursor signal of disruption and the development of an algorithm for real-time alert to predict disruptions in tokamaks applying a Singular Value Decomposition (SVD) to magnetic signals. The analysis has been applied to the magnetic Mirnov signal of the FTU and JET tokamaks. Disruptions are often accompanied by the onset of magnetic islands located on low values of q=m/n rational surfaces, where m and n represent respectively the number of toroidal and poloidal revolutions of the force lines of the magnetic field. The application of SVD to Mirnov coils signals has long been used in several tokamaks for the study of Magneto Hydro Dynamics (MHD) activity, detecting the presence of the MHD instabilities and characterizing the (n,m) mode numbers. From the application of SVD to the fluctuations of the poloidal magnetic field caught by Mirnov coils have been extracted useful markers related to the presence of instabilities and to the probability of the occurrence of a disruptive event. These markers are the entropy H that describes the phase coherence in Mirnov coils and the marker P1 related to the presence of the dominant couple (m,n). In this thesis has been identified a precursor of disruption through the study of the time evolution of the markers during the plasma discharge. This work has carried out processing 2046 FTU plasma shots and 2044 JET plasma shots. The result of the analysis is the development of a set of algorithms based on the SVD analysis of the MHD activity signals caught by Mirnov coils that provides a disruption precursor able to recognize up to 82% of the disruptions; 79% of the recognized disruptions are identified 20 ms before the current quench for the FTU tokamak and 50 ms before the current quench for the JET tokamak.

Thesis Overview

This PhD project is part of research on controlled thermonuclear fusion, it concerns the identification of a precursor signal of disruptions in tokamak devices and the development of an algorithm for real-time alert to predict them.
The controlled thermonuclear fusion offers a large and important field of research: from the socio-economical point of view for the growth of the energy requirements, from the engineering and technological point of view to the development of sophisticated experimental devices, from the physical point of view in order to study the plasma in particular temperature and density conditions. A major limitation to fusion goals is made by the onset of magnetohydrodynamic instabilities in plasmas. These instabilities if not controlled can lead to disruption, i.e. the sudden fall of plasma current followed by the loss of confinement. Disruption is very dangerous for the integrity of the reactor because the energy stored in the plasma is abruptly released to the wall machine. The study and prediction of disruption is therefore a fundamental research topic in this context. In this work, the precursor signal is determined through the analysis of the results obtained by applying a Singular Value Decomposition (SVD) algorithm to Mirnov magnetic signals. The analysis has been applied to the magnetic Mirnov signals of the ENEA tokamak FTU (Frascati Tokamak Upgrade) located in Frascati (Italy) and after that the same analysis has been adapted and applied to the magnetic Mirnov signal of the tokamak JET (Joint European Torus) Culham, UK. The present PhD research work has been supported by a scholarship financed by Politecnico di Milano, under the supervision of Prof. Gabriele D'Antona from Politecnico and Dr. Carlo Sozzi from Istituto di Fisica del Plasma IFP-CNR Milan (Italy).
Chapter 1 starts with a brief introduction to controlled thermonuclear fusion. It follows with a description of a tokamak, underlining the most important parameters in the study of stability. Then it proceeds by introducing the main magnetohydrodynamics instabilities that bring the tokamak plasma to disruption. The resulting magnetic field in a tokamak is the sum of a particular combination of a poloidal magnetic field and a toroidal magnetic field. The ratio between the number of toroidal and poloidal revolutions of the force lines of the magnetic field is define as q=m/n. Disruptions are often

accompanied by the onset of magnetic islands that arise from the development of Magneto Hydro Dynamics (MHD) instabilities. The most dangerous magnetic islands are located on low rational values of q. A brief description of the disruption and some basic about the existence of disruption prediction, avoidance and mitigation have been introduced.
Tokamak devices are equipped with different measurements and diagnostic systems in order to understand plasma physics in extreme situations, as high density and temperature. There are several diagnostics devoted to the study of plasma instabilities and MHD mode detection, the signals used in this analysis are the fluctuations of the poloidal magnetic field caught by a set of Mirnov coils. The description of the diagnostic and measurements of interest in this topic, i.e. magnetic measurements as Mirnov coils is provided in chapter 2.
The description and the application of a Singular Value Decomposition (SVD) to FTU Mirnov coils and the introduction of the physical quantities which are fundamental in this research of the disruption precursor are addressed in chapter 3.
The main parts of this thesis are chapter 4 and chapter 5 that describe the research in the identification of a disruption precursory marker and the application to the FTU and JET Mirnov coils signals respectively. Some useful markers of instabilities can be extract from SVD analysis of Mirnov signals. Among various markers, in this analysis are very useful the entropy H that describes the phase coherence in Mirnov coils and the marker P1, related to the presence and the stability of the dominant mode (m,n) in the plasma discharge. The investigation starts from the evidence that $H \rightarrow H_{min}$ where H_{min} is a value close to 0 in disruptive shots and proceeds with the analysis of the plasma discharge in the plane H-P1. The key issues of the work are the identification of markers related to the occurrence of disruption and the test that are good precursors if they maximize the number of right alarms and minimize the number of false alarms with an alarm time sufficient to take precautionary measures.
The result of the analysis carried out at FTU provide a disruption precursor able to recognize up to 82% of the disruptions and 79% with 20 ms of warning time before the plasma current quench. The analysis applied to JET machine allows to recognize up to 79% of the disruptions, at least 50 ms in advance. The results are encouraging and for the importance of the topic of research it will be useful to continue the work with further investigations as summarized in chapter 6.

Chapter 1

Introduction to Controlled Fusion, Plasma Tokamaks Instabilities and Disruptions

1.1 Controlled thermonuclear fusion

Nuclear fusion was first proposed by Eddington in 1920, to explain the energy mechanisms that support the Sun and other stars. A quantitative theory of thermonuclear fusion was advanced in 1928 by Atkinson and Houtermans to describe the rated power output of 300 Wm^{-3} in the Sun. This theory, when it was not yet known the existence of the neutron, assumed the fusion of four protons to form a α particle. Over the next decade, more detailed models explained the energy balance in the stars based on fusion reactions: the proton-proton chain and the carbon cycle. These reactions are too slow and require high density and have cross sections too small to be observed in the laboratory.
The fusion reaction that will be used in the first reactor is the deuterium-tritium reaction

$$D + T \rightarrow^4 He + n + 17.6MeV$$

given that at the same power gain, the threshold temperature is lower, less confinement is needed. Moreover, this reaction provides more power at a given plasma pressure. The energy produced in a reactor must balance the energy used to bring the reactor in fusion conditions and this principle is expressed by the Lawson criterion. For a D T reaction the Lawson criterion [8] is written as

$$n\tau_E T \geq 10^{21} keVs/m^3$$

where n is the particle density, T the temperature and τ_E the energy confinement time.
There are two different approaches to fusion: inertial confinement and magnetic confinement. In the first approach the plasma is created and compressed in a very short time ($10^{-11} - 10^{-10} s$) by bombardment with energy beams of laser light or particles of small quantities of material containing deuterium or tritium in high density ($n \sim 10^{31} m^{-3}$) until reaching fusion conditions. In the magnetic approach, particular configurations of magnetic fields are used to confine for times greater than 1 second a plasma at low density ($n \sim 10^{20} m^{-3}$) which is heated up to the temperature of ignition.
The inexhaustibility of the sources, the safety, the environmental and economic aspects make thermonuclear fusion an important and interesting field of study. The continuous demand for energy and the slow exhaustion of energy resources require the development of new technologies and researches. Research in the field of thermonuclear fusion is very challenging both from the technological point of view and from that of the study and understanding of plasma physics.

1.2 Tokamak

Tokamak is the most common configuration for the study of a magnetically confined thermonuclear plasma in which are largely concentrated the research on fusion. The name tokamak is a Russian acronym for toroidal chamber with magnetic coils (TOroidal'naya KAmera v MAgnitnykh Katushka-kh). It is an axisymmetric configuration in which there are a toroidal field produced by external coils and a poloidal field generated by a toroidal current flowing in the plasma. The toroidal field alone does not allow confinement of plasma because positive ions and electrons constituting the plasma in the presence of the only toroidal field would be subject to a drift motion in opposite directions. In order to have an equilibrium in which the plasma pressure is balanced by magnetic force it is necessary also to have a poloidal magnetic field. The combination of the toroidal field and poloidal field gives rise to magnetic field lines which have a helical trajectory around the torus. The toroidal field is produced by a set of magnetic coils surrounding the plasma, while the poloidal field is produced by the current produced by the plasma that acting as the secondary winding of a transformer and this current flows in toroidal direction [4, §1]. The schematic representations of a tokamak with magnetic field coils, magnetic field lines and currents required to confine the plasma are shown in fig. 1.2 and 1.1.
In figure 1.1 we note the presence of external coils that realize auxiliary magnetic fields for the control of position and shape of the plasma. The plasma

has the property of being a good conductor and can be heated by an induced current from the outside. In 1.1 is shown how the plasma behaves like the secondary winding of a transformer, whose primary is outside. The current creates the poloidal field and heats the plasma through the so-called ohmic heating or resistive heating. The ohmic heating alone is not sufficient to reach the ignition temperature, then are used auxiliary heating systems such as radio frequency heating and neutral beam heating.

The main goal of plasma tokamak research is to demonstrate the scientific feasibility of thermonuclear fusion. A useful and important engineering parameter is the gain, defined as the ratio Q

$$Q = \frac{P_{fus}}{P_{aux}} \tag{1.1}$$

where P_{fus} is the power produced by thermonuclear reactions and P_{aux} is the power provided by additional heating systems. The fusion reaction is self-sustaining when all losses are balanced by the heating of the plasma produced by the alpha particles P_{fus} and is no longer need to inject power from the outside. Thus, the ignition condition is reached when $Q \to +\infty$, actually Q finite (> 1) allows to gain more than what is expended [9]. For deepening knowledge, see [4, §1].
We have seen above that in a tokamak the magnetic field is the vector sum between a toroidal magnetic field B_ϕ and a poloidal magnetic field B_θ, the force lines of the magnetic field are helical and lies on isobaric surfaces. Another important parameter is β defined as the ratio between plasma pressure and the magnetic field pressure

$$\beta = \frac{2\mu_0 p}{B^2} \tag{1.2}$$

which can vary from 0 to 1 and is connected to the stability of the plasma and is a measure of how efficient the magnetic field is at confining plasma. The stability is expressed by the safety factor q. In axisymmetric equilibrium each magnetic field line has a value of q. The field lines follows a helical path as it goes around the torus on its associated magnetic surface. If at some toroidal angle ϕ the field line has a certain position in the poloidal plane, it will return to that position in the poloidal plane after change of toroidal angle $\Delta\phi$. The q value of a field line is defined as the number of times a field line on a flux surface goes around toroidally for one poloidal circuit:

$$q = \frac{\Delta\phi}{2\pi} \tag{1.3}$$

greater stability corresponds to higher values of q. An important parameter characteristic of the balance condition is the inverse aspect ratio, defined as

$$\epsilon = \frac{a}{R_0} \tag{1.4}$$

where a is the minor radius and R_0 the major radius of the tokamak. This parameter has important implication about the geometry of the machine. In the limit $\epsilon << 1$ it is possible to ignore the effects of the toroidal curvature and describe the geometry of the tokamak in cylindrical coordinates, otherwise it is necessary to introduce a description in curvilinear coordinates. In the limit $\epsilon << 1$ it is possible to use this approximation

$$q \to \frac{N_{tor}}{N_{pol}} \tag{1.5}$$

where N_{tor} denotes the number of times that a magnetic field line goes around a torus toroidally and N_{pol} is the number of times that a magnetic field line goes around a torus poloidally before joins up on itself. The safety factor is very important in the study of plasma stability. In the next subsection we will see that on the surfaces on which the magnetic lines of force of the field B have a rational step (rational surfaces) $q = \frac{m}{n}$ is rational, m and n are integers and are defined as poloidal and toroidal mode numbers. They represent respectively the number of toroidal and poloidal revolutions of the force lines of the magnetic field [4, §3].

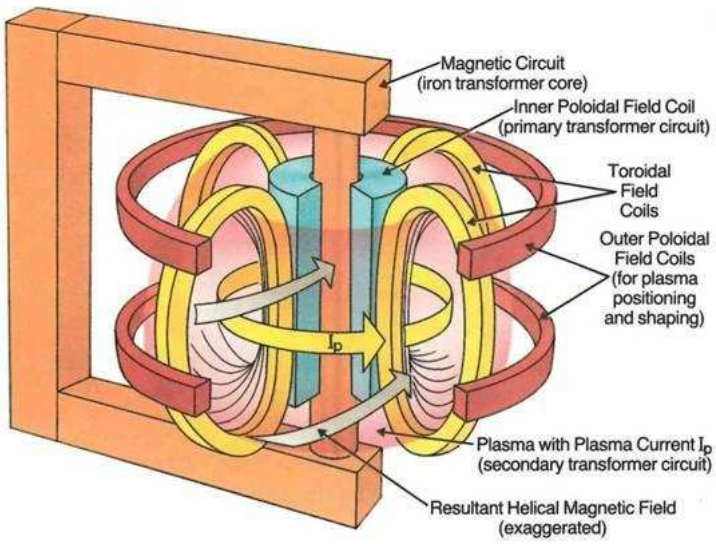

Figure 1.1: Schematic representation of a tokamak in which are in evidence: the inner poloidal field coil and the plasma current i.e. the primary and secondary transformer circuits, the magnetic circuit, the toroidal field coils and the outer poloidal field coils [1].

Over the past decades many tokamaks have been operated to investigate fusion science and its scientific feasibility for energy production. In this intro-

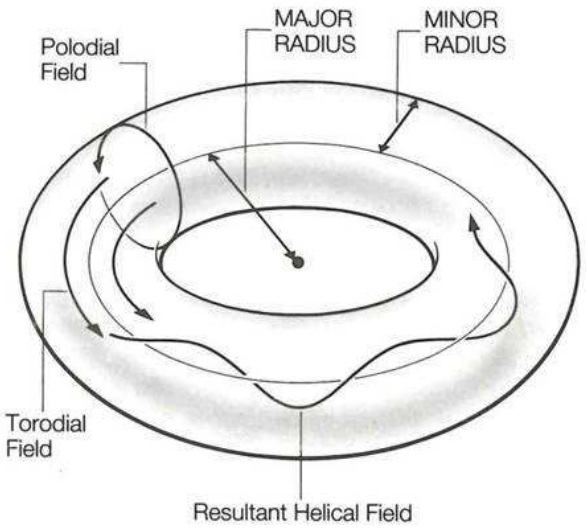

Figure 1.2: Schematic representation of the geometry of a tokamak. The Major Radius and the minor radius are in evidence. All the magnetic lines are shown: the poloidal field, the toroidal field and their combination as resultant helical field.

duction we remember project as ASDEX Upgrade in Germany, Tore Supra in France, FTU in Italy, JET in UK, JT-60U in Japan, TFTR and DIIID in the USA but many other devices have been operated all over the world. All the studies of plasma physics among these tokamaks are a fundamental contribution to ITER (International Thermonuclear Experimental Reactor) project, the ambitious fusion device with the aim to demonstrate the scientific and technology feasibility of controlled thermonuclear fusion with a significant value of Q factor. ITER project born at the end of last century from an international collaboration and the plant is under construction in Cadarache (France).

1.3 MHD instabilities and disruptions

The range of operation of tokamaks is limited by Magnetohydrodynamic (MHD) stability and by the effects of MHD instabilities. A plasma confined in a tokamak is prone to MHD instabilities that may affect the energy and confinement time of particles or lead in some cases to disruptions. Disruptions are abrupt uncontrolled events involving a sudden loss of the magnetic configuration, cooling the plasma and contaminating of impurities and are dangerous for the integrity of the machine. Disruption-free operation in a

tokamak system is limited by maximum plasma current, maximum electron density and maximum plasma pressure (β) [10]. The control of the growth of instability or identify a disruption precursor signal and develop a real time algorithm for disruption predictions is of fundamental importance because the consequences of disruptions in large tokamak as ITER are very severe. In every tokamak there is an incentive to obtain an acceptable balance between maximum plasma performance and disruption frequency but in large tokamaks there is more attention in control instabilities, avoid disruption occurrence and mitigate consequences.

1.3.1 Magnetic islands and tearing modes

The ideal Magnetohydrodynamics describes the interaction between a perfectly conducting fluid and a magnetic field. The plasma, despite being a good conductor, has a small but finite resistivity. The addition of resistivity to ideal MHD equations allows to magnetic field lines to break and reconnect in a new topology. The rational surfaces with constant magnetic flux and pressure tear, allowing to force lines of the magnetic field to reconnect and consequently creating helical magnetic islands structures. In figure 1.3 a) we can see a simple example of the reconstruction of a equilibrium profile for the FTU discharge 29473 at t=0.818 s while in b) the experimental Soft X-ray tomography in which is evident the presence of magnetic island structures. A tokamak can also operate in the presence of magnetic islands, but their evolution and the uncontrolled growth can lead to disruption. Modes of lower number are the most unstable. The most important and dangerous are those with $m/n = 3/2$ and $m/n = 2/1$.
A class of resistive instabilities are the tearing modes (TM), the tendency for the magnetic configuration of a plasma to break up into magnetic islands in order to reduce the magnetic energy in the regions away from the islands. TM occur as helical perturbations of the current and temperature of the plasma localized around the rational surfaces rapidly rotating [11]. Tearing modes instability may take place around the magnetic surfaces with low rational values of the ratio m/n, limiting the performance of a tokamak. Neoclassical Tearing Modes (NTM) arise from the modification of the bootstrap current as a result of the reduction in the temperature and density gradient which drive this current [4, §7].

1.3.2 Disruptions

Disruptions can arise as consequence of the growth of MHD instabilities and are dramatic events in which after a complete loss of current the plasma confinement is suddenly destroyed. Disruptions pose a serious problem for tokamak operations because their occurrence leads to a large mechanical and thermal stress to the wall machine. The consequences of disruptions

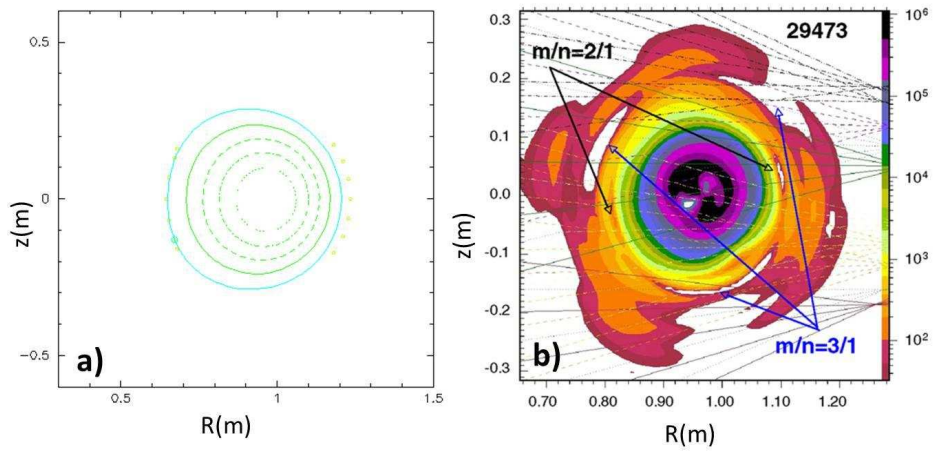

Figure 1.3: Cross section of a) equilibrium nested flux surfaces for the FTU discharge 29473 at t=0.818 s compared to (b) the experimental soft x-ray tomography with island structures for the FTU discharge 29473 at t=0.818 s [2].

are more dangerous in tokamaks of larger dimensions. In order to have a sufficient energy gain from the fusion reactions it is necessary to operate at high β value. This scheme involves working such as high current, high magnetic energy and high plasma parameters: situations in which the occurrence of disruption is inevitable and very dangerous for the integrity of the machine. Therefore minimize the numbers and the gravity, study causes and determine precursor signals that can avoid disruptions are very important research subjects.
Usually in literature with the name major disruption is indicated the sudden and uncontrolled lost of plasma confinement, while minor disruptions or pre-disruptions mean the initial step or a series of intermediate phenomena. Major disruption are preceding by a weakening of the magnetic shear in the plasma core, as consequence of the growth of instabilities or minor disruptions, locked mode or NTM development, impurity accumulation and so on. During a minor disruption the magnetic field lines fastly reconnect, without a large energy lost and current decay.
Major disruptions are classified in two main categories: density limit disruptions and low q disruptions [12]. Given a plasma current, if there is a limit to the plasma density reached without having a disruption, we have a so called density limit disruptions. The impurity radiation increases with density and this lead to a contraction of plasma temperature and to the development of MHD instabilities and as consequence a fast decay of plasma current. The low q disruptions occur if the current decay and the energy loss are due to a

growth of MHD instabilities when q reaches a critical value.
The operational limits imposed by disruptions in terms of density and safety factor are commonly represented in the Hugill Diagram [13]. The Hugill Diagram for JET tokamak is shown in figure 1.4 where q_a denotes the safety factor at the edge of the plasma and $\frac{nR}{B_\phi}$ is the Murakami parameter, where n is the plasma density, R the major radius of the tokamak, and B_ϕ the toroidal magnetic field. In fig. 1.4 plasma operation with ohmic heating alone in the shaded region are precluded by disruptions, when is used additional heating the density limit is increased as shown by the dashed line [3].

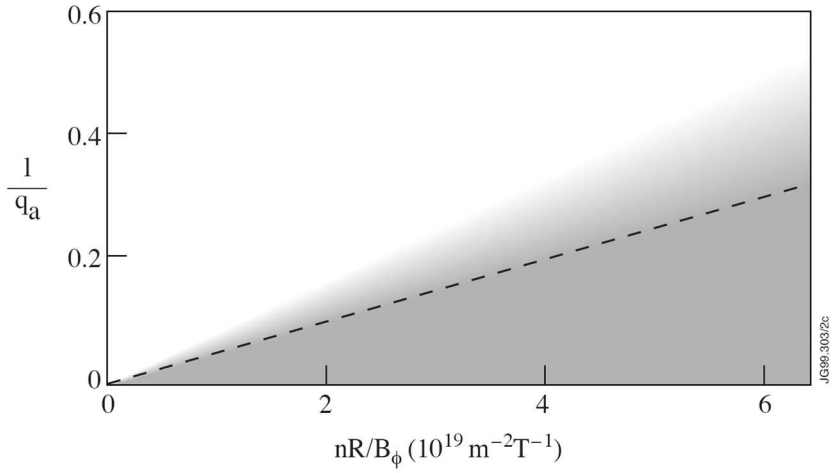

Figure 1.4: Hugill Diagram for JET tokamak [3].

1.3.3 Physics and phases of disruptions

The physical processes that cause disruptions are quite complicated and actually studied. The main causes of disruptions can be found in the evolution of unstable current profiles which lead to large amplitude tearing modes, especially the growth of an $m = 2$ mode; the existence of magnetic field errors seem to provide a seed for the growth of TM. The impurity that fall into the plasma and the development of vertical instability in elongated tokamaks also lead plasma to disruptions.
During density limit disruptions it is possible to recognize four phases:
1) Radiative contraction phase;
2) Precursor instabilities phase;
3) Energy quench phase;
4) Current quench phase.

This phase are briefly summarized as follows:

Radiative contraction

The first sequence during a density limit disruption is the radiative contraction. The impurity radiation sets a limit to the plasma density. The density rises and a fraction of heat loss transforms in radiation and thermal conductivity decreases. When is reached 100% radiation temperature and radiation profiles can contract. This contraction drives MHD instabilities in the plasma. The physics of contraction is quite complex but an exhaustive model can found in [12].

Precursor instabilities

After the start of radiative contraction magnetic oscillations appear. These magnetic oscillations have low poloidal and toroidal mode numbers and are associated with magnetic islands at the corresponding rational magnetic surfaces. The island rotates producing the oscillation in the magnetic field. The growth of magnetic oscillations are measured outside the plasma by Mirnov coils (see next chapter). A simple example of the behavior of the growth of instabilities is shown in figure 1.5. The growth of the magnetic fluctuation $\frac{\mathrm{d}B}{\mathrm{d}t}$ before the current decay is related to the growth of the associated magnetic island.

Energy quench

The energy quench (or thermal quench) is the main feature characterizing disruption and follows the initial MHD precursor growth phase. During the energy quench there is a loss of plasma thermal energy typically occurring on a timescale of several ms. The evidence for the current flattening is the observation of a negative voltage spike due to the flux change induced by the increase of plasma current, as shown in 1.6 for a FTU disruptive shot.

Current quench

At the end of a disruptive event the plasma current falls to zero in a time depending on plasma conditions. The reason of plasma decay depends by the previous plasma cooling and the consequent resistance increasing. The plasma, after the energy quench, is very cold and more resistive and the toroidal electric field provided by the ohmic loop voltage is not able to maintain the plasma current that finally decays. The cooling of the plasma during the current quench phase brings a change in plasma inductance. The change in inductance is very rapid and gives rise to the large spike in the plasma current.
The rapid decay in plasma current generates strong forces on the vacuum

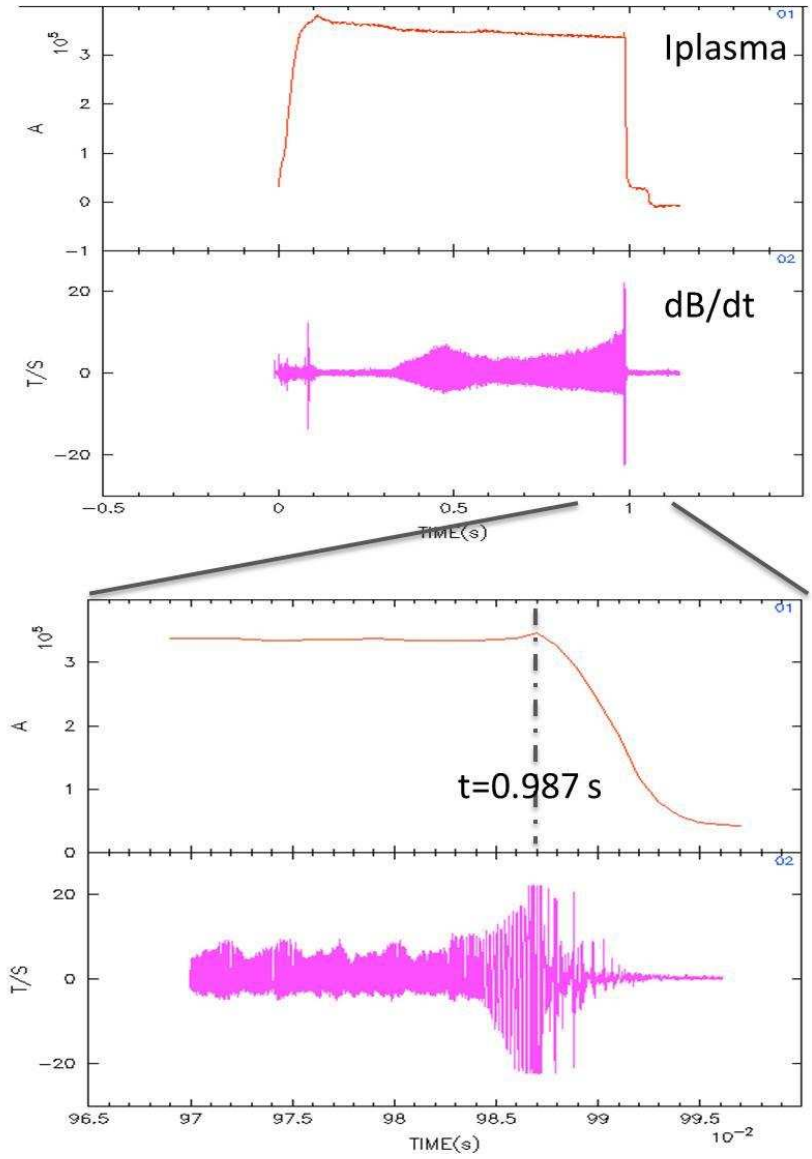

Figure 1.5: FTU plasma disruptive discharge 36252. The plasma current (red) and a simple example of Mirnov coil fluctation $\frac{dB}{dt}$ (magenta) are shown.

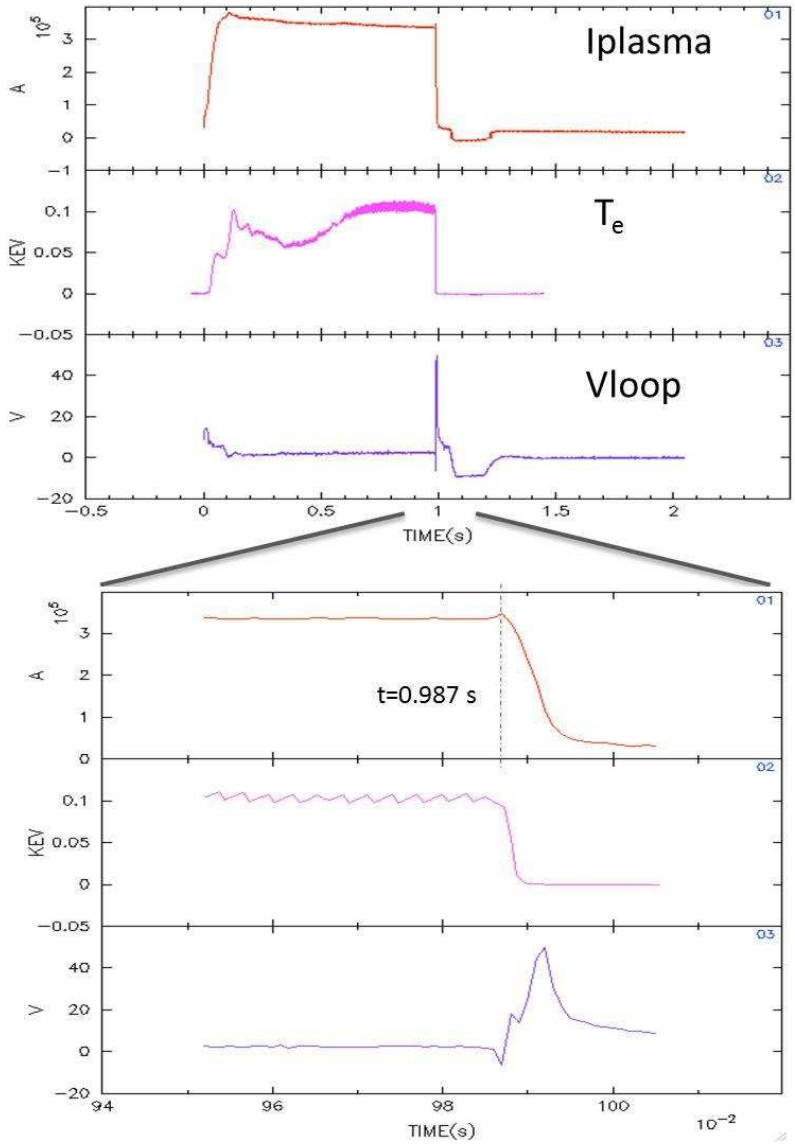

Figure 1.6: FTU plasma disruptive discharge 36252. Plasma current (red), electron temperature T_e (magenta), loop voltage (violet). Zooming in around disruption time t=0.987 s is evident that the plasma current increases, the electron temperature T_e falls and negative voltage spikes at disruption.

vessel that are very dangerous for the integrity of the machine.
The current quench phase of disruptions in elongated plasma configurations as JET is vertically unstable. Vertical instability is not itself a disruption but can lead to a disruption through the reduction of the surface q value. If the vertical control is lost the plasma moves vertically and can lead to very large currents and strong forces on the vessel. During vertical displacement events (VDEs), that commonly affect elongated tokamaks, the loss of vertical stability gives rise to halo currents. The high electric fields inherent in the current quench phase of a disruption or VDEs can convert a consistent fraction of initial plasma current in runaway electron current.

1.4 Other instabilities

In order to complete this essential summary on instabilities and disruptions, we remember also the existence of sawtooth oscillations, mode locking, error field instabilities and Edge Localised Mode (ELMs).

Sawtooth oscillation

Sawtooth oscillations are periodic MHD mixing events that occur in the centre of plasma tokamak where the safety factor $q \leq 1$. They are observed as relaxation oscillations of temperature and density visible in the central part of the plasma. The emission increases slowly, and then collapses rapidly as the instability occurs with the characteristic waveforms oscillation of temperature and density that gives the name. Kadomtsev proposed a model involved a fast reconnection of the magnetic surfaces during the instability in order to explain the rapid collapse. There is a disagreement between theory and experiment over sawtooth oscillations that are interesting argument of study.

Mode locking

A conducting wall on the vacuum vessel is able to lock a mode. In presence of finite amplitude perturbation the interaction between the plasma and the wall acts to reduce the phase velocity and the frequency of the instabilities. This phenomenon bring to an abrupt halt of oscillations. Figure 1.7 shows a time trace for a case where the plasma is slowed and halted. The magnetic signal gives the frequency and growth of MHD instability. The reduction in frequency shows the slowing down of the plasma rotation. The signal measures the time rate of change of the magnetic field as seen by a coil outside the plasma, the removal of a huge part of oscillation indicates the final mode locking. The magnetic signals rotates with the plasma thanks to its high electrical conductivity. The perturbed magnetic field extends to

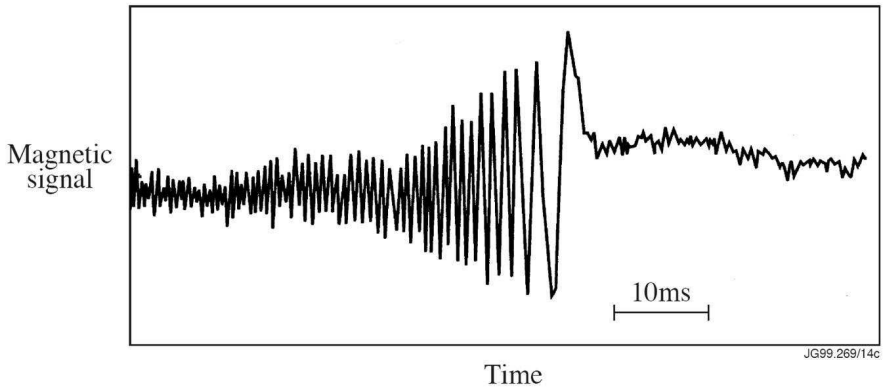

Figure 1.7: Magnetic signal shows the frequency and the growth of MHD instability. The reduction in frequency corresponds to a fall of the velocity, the removal of the gross oscillation indicates the final mode locking [4].

the conducting material surfaces surrounding the plasma that are not highly conducting. As the instability grows the drag increases and the plasma is brought almost to a stop. In presence of mode locking, it is generally no more possible to stabilize the mode and it will grow until the lose of confinement. For this reason mode locking constitute a significant limitation on the operational parameters achievable in tokamaks [3].

Error field instabilities

Small deviations from toroidal symmetry introduces perturbing components to the magnetic field and can lead to the growth of the $m = 2$ modes. Error field instabilities can arise from the internal winding structure of coils, from the connections to the coils and from misalignment of the coils. Errors field are related to the saturation of island width and it is clear that reducing their magnitude avoid disruptions. Larger tokamaks can be more sensitive to mode locking and error fields since the susceptibility of plasma tokamaks to error field induced mode locking seems to increase with major radius and with toroidal field. The study of tolerability for error fields and avoiding mode locking are fundamental issue for future reactor tokamaks.

ELMs

The transition from low confinement mode (L-mode) to high confinement mode (H-mode) in tokamak operations is accompanied by the observation in the H-mode phase of periodic Edge Localized Mode of instabilities (ELMs). These instabilities, detected by magnetic pick up coils and soft X-ray diodes,

causes a reduction in density and temperature in the outer zone of the plasma and the periodic behavior constitutes a relaxation oscillation followed by the consequent lost of confinement [4, §7].

1.5 Disruptions causes and classification

Disruptions can occur in different regions of the plasma and arise from different conditions, for these reasons the definition of a precursor is not univocal and its definition is often based on the statistical data analysis on the experience of several years of plasma operations. The research of disruption causes contributes to define better strategy to mitigate or prevent their consequences. A recent survey of disruption causes at JET has been carried out in [14]. Although different tokamaks don't operate in the same operational range, the results of this survey on JET could be seen as quite representative for the general operations of a large tokamak. This paper has taken into consideration 2309 intentional and not intentional JET disruptive plasma discharges in the previous decades (2000-2010). Often the events that lead to a disruption are a complex combination of several destabilizing factors, as MHD instabilities, radiation instabilities at the edge, vertical instabilities. Moreover a highly complex pattern of chain of events led to disruption. Taking in account not only the physics instabilities that lead to disruption but also the sequence of events and the root causes, the main results are that all disruptions at JET have been eventually pushed close to an operational limit resulting in the onset of physics instabilities that for unintentional disruptions are: edge radiation instabilities, mode locking, growth of internal kink modes, vertical position instability and too low a safety factor. Considering the root causes that initiate the chain of events the main root causes of JET disruptions is due to neoclassical tearing modes (NTM) followed by human error or operational mistake. Technical and human mistakes introduce a non physics factor to the occurrence of disruptions. Reducing the disruption rate in tokamak experiments requires to understand more deeply the physics of the phenomenon and at the same time prevent operator errors.
In 2011 started at JET operations with a new part Beryllium and part Tungsten ITER-like Wall (ILW). The introduction of the new ILW leads to the need to revise the operational scenarios and the control schemes valid for the old carbon-wall. After this installation the disruption rate, i.e. the fraction of discharges that disrupt unintentionally, increases to 10% [15]. A survey similar to the analysis for the previous carbon-wall operations has been carried out identifying the dominant cause of disruptions during the 2011-2012 ILW operations in high levels of high-Z impurities and high core radiation [15].
The comparison of the disruption classification system reported in [15] with a different device is useful in order to formulate universal criteria for dis-

ruption avoidance and prediction. The same classification system has been applied, when possible, to the classification of disruption causes in ASDEX Upgrade [16]. The same classification of disruptions developed for JET results to be valid also in ASDEX, with a different occurrence percentage for each class of disruption. This fact is dependent on the different heating systems, competences and experimental campaigns between the two the devices.

1.6 Disruption prediction, avoidance and mitigation

This section reports a review of method and technique to predict and avoid disruptions or mitigate their consequence. In literature [10], [17] are present several approaches to disruption studies and can divided into three groups:
1) investigation and implementation of a reliable real-time disruption prediction or an advance warning method in order to avoid the occurrence of disruptions;
2) intervention to avoid the growth of instabilities before the thermal quench;
3) mitigation and amelioration of the effects, to reduce the severity and the consequence of disruptions.
Among the techniques of prediction we remember statistical methods, as artificial neural networks and support vector machine (SVMs), that are computational systems capable of building general models, by learning from the data, the so-called training process [18]. By detecting significant patterns in the available data, a computational system based on machine learning concepts can take decisions or make predictors about new data coming from the same physical source. It is worth mentioning the Advance Predictor Of DISruption (APODIS) [19] implemented in JET's Real Time Data Network, a project started in 2008 with the aim of developing a disruption predictor for JET that overcomes the problems of earlier predictors [20]. APODIS in an engineering system able to learn from past situation, rather that a system related to the investigation of physics causes.
A possible method, largely used at FTU, for disruption control aiming at disruption avoidance is given by the use of the electron cyclotron resonance heating (ECRH) [21]. This method consists in the additional heating of the plasma through the absorption by electrons injected int the plasma with electromagnetic waves at electron cyclotron frequencies.
While all the techniques for disruption avoidance and mitigation are being tested and contribute with some degree of successes, the strategy for disruption avoidance and/or mitigation in large size tokamaks is subject of active research. Disruptions occur operating in high performance conditions, therefore it is important to classify them on the one hand, on the other hand anticipate their occurrence. For this reason the definition of a precursor signal of disruption is currently a interesting argument of research and in this

thesis a method to derive a real time signal precursor of disruption is proposed proposed through the analysis of the results obtained by applying an Singular Value Decomposition (SVD) algorithm to Mirnov magnetic signals.

1.7 Summary

We have begun the chapter with a brief introduction of thermonuclear fusion and a short description of the tokamak, the most studied device for magnetic confinement. Then we have introduced the MHD instabilities that lead to disruption, basic argument of the thesis. Moreover we have reviewed the operational limits of plasma tokamak, the physics and the causes of disruptions and the technique to predict, avoid and mitigate them.

Chapter 2

Measurements and Diagnostic Systems

2.1 Introduction

The experiments involving fusion plasmas confined in tokamaks, require special physical conditions such as high density and temperature, and to operate within confined magnetic fields. Diagnostic systems present in a tokamak are designed to solve several tasks. They are very complex and consist of several measuring instruments that can provide information on the plasma parameters of interest. Tokamaks are equipped with several categories of diagnostics. The diagnostics can be categorized by the parameters they measure or by experimental technique. Since different diagnostics can measure the same parameter, it is more useful categorize diagnostics by measured quantities and in this way we can distinguish: magnetic measurements, plasma particle measurements, electromagnetic emission from bound or free electrons, neutral atom diagnostics and much more [22]. Since the topic of this thesis concern MHD instabilities, in this chapter the main diagnostics used in this research area of research are shown.
In the previous chapter we have underlined the necessity and the importance in researching and improving the knowledge in MHD activity. The main tokamaks like JET or FTU are equipped with a wide range of diagnostics which are suited to the study of MHD instabilities and disruptions. The identification of MHD perturbations in the present thesis deals with timing signals associated to oscillations of the magnetic field (Mirnov oscillations). In the following sections we illustrate the operation of magnetic diagnostics and then some mention of the main non magnetic diagnostics for MHD detection.

2.2 Magnetic diagnostics and Mirnov coils

Magnetic measurements are important for the analysis and the control of MHD instabilities, but also provide real time data to measure and control the current, the shape and the position of the discharge. Magnetic measurements are fundamental and essential in plasma fusion research. Magnetic diagnostics are external to the plasma volume and passive. The measurements are valid over the full range of plasma and temperature and during such events as disruptions [5].
It is useful to introduce the expression of the magnetic field $\vec{B}$ measurable outside the plasma. In an axisymmetric configuration as the tokamak, in a cylindrical coordinate system (R, ϕ, Z) the magnetic field can be expressed in term of two scalar function F and ψ as [5]

$$\vec{B} = R^{-1}(F\hat{\phi} + \nabla\psi \times \hat{\phi}) \tag{2.1}$$

where $\hat{\phi}$ is a unit vector in the direction of symmetry and

$$RB_\phi = F \tag{2.2}$$

is the toroidal field strength, while

$$RB_\theta = |\nabla\psi| \tag{2.3}$$

the poloidal field. The easiest and diffused method to make a measurement of the magnetic field in a given point is the use of coil as probes. Here we follow the same terminology of [5] where a loop is a single closed turn of a conductor, a coil is a series of many loops and a magnetic probe is a coil that makes a local measurement of the magnetic field. The term *inductive sensors* indicates different forms of inductive loops measuring the voltage induced by a variable magnetic field. A schematic view of the common inductive sensors used in fusion device in shown in figure 2.1.
The physical principle is very simple, being Φ the magnetic flux linked by an inductive sensor, according to the Faraday's law, the voltage difference V at the terminals of a conducing loop is equal to the rate of change of the magnetic flux Φ that is linked by the loop

$$V = -\frac{d\Phi}{dt}. \tag{2.4}$$

The magnetic flux is determined by the integration of the voltage signal from the loop. Coming back to the figure 2.1 we see briefly how these inductive sensors operate and which parameter measure.
The *Rogoswski coils* are the most diffused diagnostic for plasma current measurements. They consist of toroidal coils whose axes forms one or more complete loops around the current to be measured. In condition of small

diameter and small spacing between turns respect to the gradient scale of the local magnetic field, the current linked by the coil I can be extract from $\Phi = \mu_0 nAI$ where n is the number of turns per unit length and A is the cross sectional area of the coil [22], [5].
A *diamagnetic loop* is a loop that links the plasma column, ideally locate in a poloidal plane in order to minimize coupling to the poloidal field. Diamagnetic loop is used to measure the toroidal magnetic flux for the purpose of estimating the thermal energy of the plasma.
A *flux loop* is simply axisymmetric loop for poloidal flux measurements, useful for plasma control and equilibrium reconstruction.
A *magnetic field probe* is a small coil measuring one component of the magnetic field strength, used in plasma control, equilibrium reconstruction and detection of MHD instabilities. The total flux linked by a magnetic probe is $\Phi = NAB_{\|}$ with N the numbers of the turns in coil, A the area of the coil and $B_{\|}$ the local magnetic field component along the axis of the coil. The high frequency fluctuations caused by plasma instabilities can be measured by the unintegrate voltage $-V = d\Phi/dt = \omega NAB_{\|}$ where ω is the frequency of the fluctuation. Usually sensors measure fluctuations in the direction tangent to the surface and perpendicular to the toroidal direction, in the poloidal plane.
A *Saddle loop* consists of a large single turn or multiturn coil in a roughly rectangular shape, mounted on the vacuum vessel wall or other structure near the plasma. The dimension of a saddle loop are intermediate between a flux loop and a magnetic probe. A saddle loop can work both as a magnetic probe then as a measure of flux difference. Saddle loops are used for equilibrium reconstruction data and for detecting non axysimmetric fields caused by nonrotating MHD instabilities [5].
The ideal location of inductive sensors for the diagnosis of fast events is inside the vacuum vessel, in order to avoid its electromagnetic shielding.

2.2.1 Magnetic measurements and MHD mode detection

The most widely used diagnostic for the detection and the classification of MHD instabilities is an array of small magnetic loops. The Russian scientist S. V. Mirnov was the first to use arrays of multiturn coils oriented to measure the poloidal component of the magnetic field, the so called Mirnov coils [23]. An array of Mirnov coils is a suitable tool for detection and analysis of mode structure, thanks to the possibility of measuring the time evolution of the magnetic field perturbation along the torus. Mirnov coils can detect instabilities in a frequency range from a few Hz up to few hundreds of kHz.
The oscillatory magnetic signals are the time derivative of the poloidal magnetic field at the edge of the plasma as measured by the voltage induced in a pick-up coil.
In Chapter 1 has been shown that the reconnection of magnetic surfaces

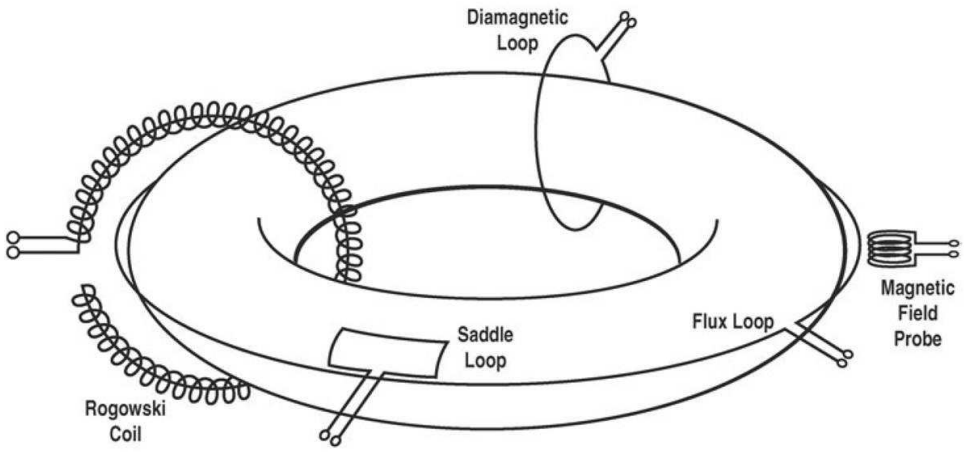

Figure 2.1: Schematic figure of a toroidal plasma showing inductive sensors and Rogowski coil [5].

forms magnetic islands localized in the plasma. The magnetic perturbation is detectable outside the plasma with the Mirnov coils. The instabilities rotates toroidally and through magnetic measurements at different toroidal and poloidal positions it is possible to determine the structure, the amplitude and the frequency (Fourier analysis) of the magnetic perturbations. The spectrograms of magnetic probes signal, generated by the Fourier analysis on successive short time windows, show the time evolution of the amplitudes and frequencies of several tearing modes [5]. In figure 2.2 is shown a spectrograms and mode analysis for FTU shot 36252.
The use of coils allows to detect perturbations at the plasma edge with small amplitude. Instabilities usually rotates and magnetic coils detect the time derivative of the magnetic field even when magnetic perturbations are only 10^{-4}-10^{-3} of the equilibrium field. Stationary perturbations as mode locking can be detect using an appropiate combination of several coils so as to eliminate the equilibrium field. In addition, usually mode locking occurs when the instabilities have grown in amplitude, making easier the detection [4, §10].

2.3 Non magnetic diagnostics for MHD detection

It is worth to mentioning other routinely used non magnetic diagnostics in the study and the observation of MHD instabilities.

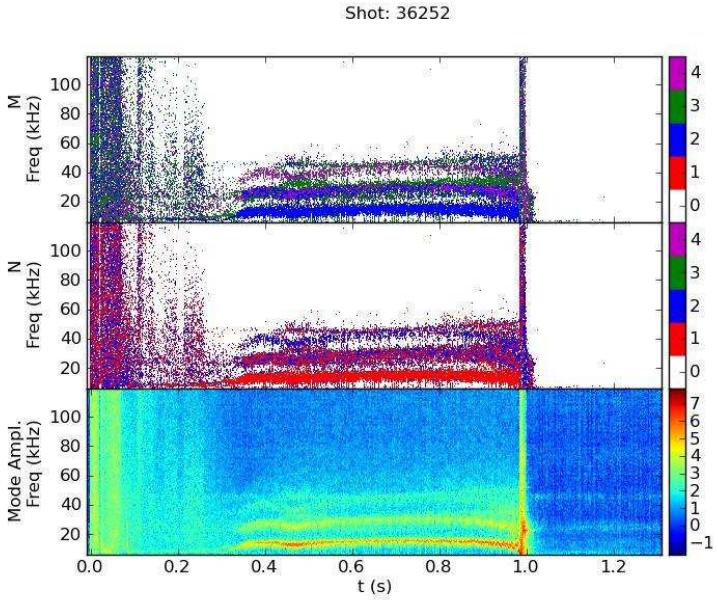

Figure 2.2: Spetrogram of magnetic probe signals in FTU, showing the time evolution of the frequencies of several tearing modes for the shot 36252. The mode numbers are obtained from other analysis. Bottom: frequencies and development of tearing modes; middle: n values; up: m values. The color scale on the rights indicates different value for n and m.

Electron Cyclotron Emission

The Electron Cyclotron Emission (ECE) is a widely used diagnostic tool in tokamak for spatial distribution of plasma electron temperature $T_e(r)$ measurements. A plasma in fusion conditions is fully ionized and composed by electrons and ions. The plasma is subjected to forces induced by the electromagnetic field, generated by charges and currents internal and external to the plasma. In the presence of an external magnetic field, the plasma behaves like an anisotropic and inhomogeneous dielectric medium. The motion of gyration of the electrons around the magnetic field lines takes place with discrete angular frequency $\omega = n\omega_{ce}$ and accelerated along spiral trajectories. They emit electromagnetic energy in n harmonics of the cyclotron frequency [24], [25]. The cyclotron frequency is $\omega_{ce} = \frac{eB}{m_e}$, where e is the electron charge, m_e the electron mass and B the magnetic field. Moreover, in a tokamak the magnetic field varies with the inverse of the major radius $B \sim 1/R$. The emission of radiation at the second harmonic in the extraordinary polarization is directly proportional to the plasma electron temperature, for plasma with high temperature and density [24]. ECE diagnostics provide a good spatial (a few cm) and temporal resolutions (down to microseconds). If the plasma is optically thick in a large enough frequency interval, while the magnetic field varies monotonically trough the plasma, electrons at different radial position emit at different frequencies: from the relationship between frequency and plasma radius, the temperature profile can be obtain directly from a measurements of the ECE spectrum. Different instruments are applied for measurements as Michelson interferometry, Fabry-Perrot interferometry, grating polycrhomator, eterodyne receivers and many others. Through these various instruments it is possible to reconstruct the temperature profiles. The ECE Mirnov cross-correlation provide information on the instability presence and on its location. The instability position can be evaluated in real time calculating the amplitude and the phase of the local T_e fluctuations by applying, for example, a dual phase lock-in algorithm [26] to signals coming from ECE and from Mirnov diagnostics.

Soft X-ray (SXR)

The bremsstrahlung radiation in a ionized plasma arises from the scattering of free electrons by plasma ions. This emitted radiation in a fusion plasma takes place in the Soft X-ray (SXR)[1] energy domain. The bremsstrahlung emissivity per unit volume per solid angle per unit frequency can be written

[1] A plasma emits electromagnetic radiation due to a variety of interaction process between electrons, ions and not fully ionized atoms, in a energy range equivalent to the temperature of the plasma from a few to several keV. The electromagnetic radiation between 100 eV and 10 keV is called Sof X-ray (SXR) radiation.

as [27]

$$\epsilon_\nu = 5.0 \times 10^{-54} \frac{n_e^2 Z_{eff} g_{ff}}{\sqrt{T_e}} e^{-h\nu/T_e} \ (Wm^{-3}sr^{-1}Hz^{-1}) \qquad (2.5)$$

where n_e is the electron density, T_e the electron temperature, $h\nu$ the photon energy, Z_{eff} the effective charge of the plasma and g_{ff} a quantum mechanical correction factor. Spatial plasma perturbations that locally change T_e or n_e such as sawteeth oscillations or MHD modes cause a significant change in SXR emission.
The SXR emissivity can be detect along line of sight, and spatially information about the perturbations can be obtained by tomography if a sufficient number of lines of sight are available. SXR are usually detect by silicon diodes characterize by an extremely fast response, typically less than one microsecond. Also pinhole cameras with more than 100 sensors viewing the plasma from orthogonal directions are used, with an excellent spatial and temporal resolution. This diagnostic has been applied to the study of sawtooth oscillations, disruptions and MHD modes [4, §10].

2.4 Summary

In this chapter we have introduced the main magnetic diagnostics used in plasma tokamaks and we have described the Mirnov coils, which have been used to collect experimental data elaborated in the analysis, as shown in the next chapters. In addition, to complete the overview of the main diagnostics used in this research area, we have introduced ECE and SXR diagnostics.

Chapter 3

Application of SVD Algorithm to Mirnov Coils

In this work the precursor signal of disruption is determined through the analysis of the results obtained by the application of a Singular Value Decomposition (SVD) algorithm to magnetic Mirnov signals.
This chapter provides a brief description of the SVD algorithm and an example of application to FTU Mirnov coils.

3.1 Mathematical background

We briefly illustrate the mathematical basis for understanding the application of singular value decomposition to magnetic signals. A signal sampled at multiple M space positions and multiple N time instants can be decomposed through a biorthogonal decomposition [28]. Consider the sampled signal as written in a matrix form as follows:

$$(Y)_{ij} = y(x_j, t_i) \tag{3.1}$$

with $i = 1...N$ and $j = 1...M$.
The decomposition of this signal is sought into a set of orthogonal time and spaces series

$$(Y)_{ij} = \sum_{k=1}^{K} A_k \phi_k(x_j) \psi_k(t_i) \tag{3.2}$$

where

$$(Y)_{ij} = \sum_{i=1}^{N} \psi_k(t_i)\psi_l(t_i) = \sum_{j=1}^{M} \phi_k(x_j)\phi_l(x_j) = \delta_{kl} \tag{3.3}$$

and

$$K = min(M, N) \tag{3.4}$$

providing a separated temporal and spatial description of the sampled signal. This decomposition can be computed through a singular values decomposition of the matrix $(Y)_{ij}$ written as follows:

$$(Y)_{ij} = VSU^T \tag{3.5}$$

where V is an $N \times M$ orthonormal matrix, S is a diagonal $M \times M$ matrix and U is a $M \times M$ orthonormal matrix. Expanding the previous matrix product it is clear that the the column of the matrix V and the columns of the matrix U are respectively the ψ_k functions and the ϕ_k of equation 3.2 while the diagonal values of matrix S are the coefficients A_k of the same equation. It is thus clear that the singular value decomposition of the matrix Y is a mean to obtain its biorthogonal decomposition. Columns of matrix VS are called *principal components* and describe the common temporal evolution of the signal as seen from the different sampling positions. Columns of matrix U are called *principal axes* and describe the spatial composition of the signal. They can be though as a still picture of the evolving signal taken from all sampling positions.
The SVD technique has the advantage that, in practice, most of the singular values are very small compared to the few dominants one. For this reason SVD is well known in the context of signal processing as noise-filtering technique [29]. The important physical parameters that one can extract from this mathematical technique are [30], [31] the global signal energy

$$E = \sum_{i=1}^{N} \sum_{j=1}^{M} (Y)_{ij}^2 \tag{3.6}$$

which is equal to the sum of its singular values

$$E = \sum_{k=1}^{K} A_k^2 \tag{3.7}$$

The dimensionless energy

$$p_k = \frac{A_k^2}{E} \tag{3.8}$$

with the property of probability distribution

$$0 \leq p_k \leq 1 \; and \; \sum_{k=1}^{K} p_k = 1 \tag{3.9}$$

and it will be shown later that these are very useful indicators of MHD activity and so interesting precursor of disruptions. We have seen in the previous sections that MHD perturbations can be seen as rotating perturbation located across helical magnetic field lines on rational flux surfaces and the

periodic magnetic field perturbations are caught by Mirnov coils. A single mode perturbation signals caught by a Mirnov coil can be written as

$$Y_k(t) = A_k \cos(\theta_k - 2\pi\nu t + \Theta) \tag{3.10}$$

where θ_k is a phase shift which depends from the mode topology and from Mirnov coil location in the tokamak, ν is the temporal frequency of rotation of the mode and Θ is a phase shift common to all Mirnov array which can be neglected if the signal of one coil is taken as reference. In the case of M Mirnov coils located at equispaced positions in a poloidal cross section of the tokamak, the phase shift becomes:

$$\theta_k = \frac{2\pi m}{M(k-1)} \tag{3.11}$$

where m is the poloidal mode number of the rotating mode. If a signal of this kind is a SV factorized the resulting first two principal axes are sinusoidal functions that mimic the above phase distribution. Counting the number of zero crossing of these principal axes and dividing by 2 yields the mode number m. In reference [31] is shown the extension to uneven spatially distributed coils and the details of the application to FTU machine Mirnov coils to obtain markers of mode structure and triggers to control action.
In reference [29] we can find the application of SVD technique to the analysis of JET Mirnov coils and in [30] of Tore Supra Mirnov coils, while in the next section it is shown the application to FTU.

3.2 Application to FTU Mirnov coils signals

The SV factorization has been applied to FTU Mirnov coils signals and presented mainly by C. Marchetto in [32], [33] e [34] and by C. Galperti [31]. The activity carried out during the PhD, presented in detail in chapter 4, is a prosecution of these works, while in chapeter 5 is shown the application to JET Mirnov coils signals.
FTU tokamak is equipped with 57 Mirnov coils installed at 6 different toroidal and 34 poloidal positions just inside the ports behind the toroidal limiter structure and the poloidal limiter [35], [32]. Each coil is composed of loops with a diameter of 33 cm. Mirnov coils are not disposed uniformly along the poloidal and toroidal direction, moreover poloidal coils are situated at poloidal angles which can differ by up to 30°while toroidal coils are situated at poloidal angles which can differ by up to 180°. Before SV factorization the raw signals from Mirnov coils (12 channels) must be preprocessed following these steps:
1) Anti alias filtering: the analog signals from Mirnov coils must be low-pass filtered (**Anti alias filters**) to avoid aliasing effects. Moreover the filter reduces the electronic noise provide by the analog chains which comprise

isolation transformers and amplification units).
2) High pass filtering: the output signal from anti alias filter is digitalized by an ADC at 100 kHz and then filtered by a high pass filter (**HIGHPASS**). The high pass filter is used in order to eliminate the bias in such a way that all signals have zero time average.
3) Signal normalization: in order to obtain that all the Mirnov coils have the same sensitivity to magnetic perturbations it is necessary to normalize the output signal from high pass filter (**NORM**). This normalization is chosen so as to obtain normalized singular values.
Since SV factorization works on set of data, time windowing (**time windowing**) is applied on sets of data. SV factorization is performed on-line on signals windows. A built in downsampling action is present in SV factorization since provided result are related to the whole time window introducing a N times downsampling (N=100 number of samples in time windows).
Given an array of signals sampled at multiple M space positions (channels) and multiple N time instants, the SVD algorithm computes a set of M scalars called Singular Values (SV), which show the possible presence of modes and weight of each of them. For every SV it provides an M dimensional vector called Principal Axes (PA) and N-dimensional vector called Principal Component (PC) which describes its mode number (m,n) and time evolution, respectively. The relevant MHD markers that can be extract are:
1) Likelihood $Ln_{n,m}$, a useful indicator to classify the mode topology, i.e. the m,n spatial structure of the MHD perturbation. $Ln_{n,m}$ evaluates how much the spatial structure of the experimentally detect perturbation is close to a perfect helical m,n perturbation. The information provides by $Ln_{n,m}$ are not enough to take measures of control and mitigation, because it does not appear to be an indicator of instability [31].
2) Singular values Entropy H

$$H = \frac{-\sum_{k=1}^{M} \frac{SV_k^2}{M} \log(\frac{SV_k^2}{M})}{\log(M)} \tag{3.12}$$

The entropy H is proportional to the square of the normalized singular values and describes the phase coherence in Mirnov coils. From 3.7 and 3.8 H is bounded between 0 and 1. $H \to 0$ indicates more instabilities.
3) $P1$ and $P2$ markers

$$P1 = \frac{SV_1^2 + SV_2^2}{\sum_{k=1}^{M} SV_i^2} \tag{3.13}$$

$$P2 = \frac{SV_3^2 + SV_4^2}{\sum_{k=3}^{M} SV_i^2} \tag{3.14}$$

These two indicators are the relative square magnitude of the two first couples of principal axes, they are bounded between 0 and 1. P1 is related to the presence of the first mode, i.e. the dominant couple (m,n), while P2 is

related to the presence of the second mode. More they are close to 1, more the first mode and/or the second mode is unstable. Usually the dominant mode at FTU is m=2, n=1 but sometimes can be m=3, n=2. As described in chapter 1, the presence of a mode indicates the growth of MHD activity, if the mode becomes unstable can occur disruption.
Data postprocessing is performed on SVD output and finally markers digital low-pass filtering (**LOWPASS**) is applied to provide suitable stable data to subsequent controllers block. All data processing computation time is less than 300 μs (with a sampling rate of 100 kHz, 100 samples data windowing and 12 Mirnov coils channels sampling) enabling real time SVD signal decomposition at output rates of 1kHz.
Figure 3.1 presents all the steps described above.
The markers extracted from SV decomposition are good indicators of the

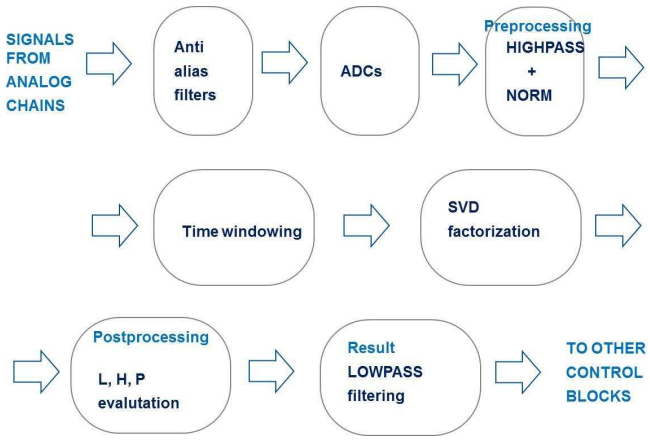

Figure 3.1: Data path of the implemented real time version of the presented analysis technique.

presence of MHD instabilities. In the next chapter is shown how these indicators can be included in an algorithm for disruption predictions.
We have seen that the SVD technique is used in fusion research in many tokamaks as JET, Tore Supra, FTU and at FTU the application to magnetic signals from Mirnov coils for mode analysis (m,n). The originality of this work is the application of SVD to Mirnov magnetic signals for FTU tokamak in order to determined a precursor and a real time alert signal of disruption. The analysis has been extended to JET tokamak.

3.3 Summary

In this chapter we have seen that given an array of M magnetic signals with N time samples, the SVD algorithm computes a set of M scalars called Singular Values (SV) which show the presence of instabilities and define some indicators that are critical in the research of the precursor of disruption. We have introduced the entropy H and the marker P1, whose use is shown in the next chapters.

Chapter 4

FTU Data Analysis

This chapter and the next one are the main part of the thesis work. The aim of this thesis is to identify an indicator with a physical meaning that is able to recognize a disruptive event. Once the indicator has been found, the next step is the development of an alert algorithm to predict disruptions in tokamaks, with the idea to implement the algorithm in real time. This work has been developed in collaboration with the Istituto di Fisica del Plasma (IFP-CNR) in Milan and has been applied both to the tokamak FTU and JET (for JET see the next chapter). In this chapter a description of the analysis carried out at the Frascati Tokamak Upgrade FTU is given.
We have seen in the previous section that the SVD technique is used in fusion research in many tokamaks as JET, Tore Supra, FTU. We have seen at FTU the application to magnetic signals from Mirnov coils for mode analysis (m,n). The originality of this work is the application of SVD to Mirnov magnetic signals for FTU tokamak in order to determine a precursor and a real time alert signal of disruption. In chapter 1 has been shown that exist many methodologies for disruption predictions, avoidance and mitigations. It is important to underline that disruption prediction is a fundamental pre requisite to put into operation any avoidance or mitigation technique. The design of disruption predictors mainly takes into account the achievement of predictions, right alarm (RA), with high success rate, low false alarm (FA) rate and enough anticipation time to act.

4.1 FTU Frascati Tokamak Upgrade

Frascati Tokamak (FT) Upgrade (FTU) is a medium size tokamak with a circular cross section. It is situated in Frascati (Italy) and it is operative since 1989. The major radius is $R_0 = 0.935\ m$ and the minor radius is $a = 0.305\ m$. FTU is an high magnetic field device, characterized by a large current density value $j \propto \frac{B}{R}$ [6], [36]. Being a high magnetic field compact tokamak it has the advantage of producing thermonuclear grade plasma at

high plasma density, low impurity concentration and relatively low beta so that it is possible to operate with high MHD limits. The aim of FTU research program are to develop relevant scenarios for burning physics experiments and improve in general physics understanding.
The main parameters of FTU device are summarized in table 4.1 while a picture of the machine is in figure 4.1. The magnetic field is produced from circular nitrogen-cooled magnetic coils. The magnetic flux is generated from an air-core transformer. The plasma shape is circular and is defined by poloidal and toroidal limiters.

Parameters	value
Major radius (m)	0.935
Minor radius (m)	0.305
Toroidal B field (T)	8
Plasma current (MA)	1.6
Max flat top duration (s)	1.6
Temperature of the first wall (°C)	-100
Repetition time (min)	20
Maximum central density (m^{-3})	4x10^{20}
Maximum electron temperature (keV)	15
Maximum energy confinement (s)	0.12

Table 4.1: Main physical parameters of Frascati Tokamak Upgrade.

4.2 FTU data analysis

In this work the database of experimental results of FTU between 2008 and 2012 has been analyzed. The database contains the results of several experimental campaigns. Some experiments are devote to the study of MHD activity that has been intentionally caused, for example, by the neon injection into the plasma [37]. For this analysis 2046 plasma shots has been selected from the whole variety of experiments and analyzed. Among these plasma shots were identified 381 disruptions and 1665 regular terminations. The 2046 plasma shots selected for the analysis are chosen if reached a stationary state characterized by a plasma current plateau with a mean value greater than 200 kA. No plasma parameter as density, magnetic field or plasma current has been considered to select the data.
For disruptive shots, the disruption time is define as the plasma current quench time t_{CQ}. This parameter is computed by the comparison with the measured plasma current and pre-programmed current and by means of moving average of plasma current derivative $\frac{dI_p}{dt}$. If $\frac{dI_p}{dt}$ exceeds a suitable threshold at time t_{CQ} disruption event is recognized [38]. Pre-programmed

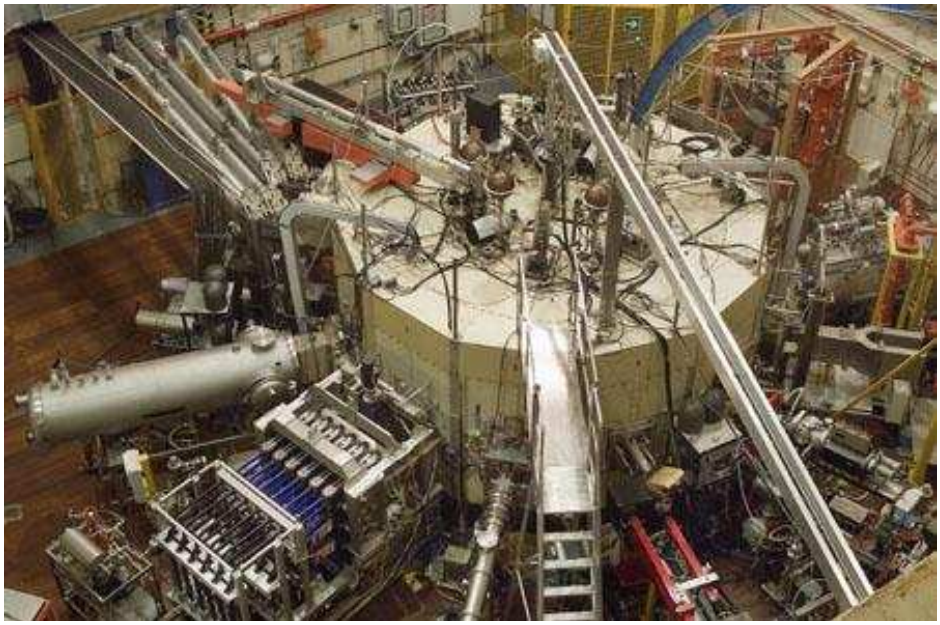

Figure 4.1: FTU machine [6].

current is defined as the current that is expected to use in every single plasma experiment.

The raw signals used in this analysis are acquired from FTU standard diagnostics, particularly magnetic fluctuations signals from the Mirnov coils system. The raw data are acquired with dedicated analog-to-digital converters and elaborated using specifically developed algorithms in order to detect the presence of the MHD activity, to track its radial position, to characterize its poloidal and/or toroidal mode number and to switch on the corrective or mitigating action as for instance powerful EC (Electron Cyclotron) waves injection. The analog signals from coils Mirnov FTU are filtered through low-pass filter and sampled at a sampling rate of 100 kHz. In the preprocessing data step the channels Mirnov sampled are first high-pass filtered then normalized. The code SVD has been online tested with a postprocessing sampling of 1 ms. In this analysis have been used 12 signals from Mirnov coils system, the typical configuration of the coils used in this work is shown in figure 4.2. This system provides the fluctuation of the poloidal magnetic field as shown in figure 4.5. In the present work the SVD code has been applied on offline data, all the computations and routines have been developed in MATLAB. The offline simulations are carried out simulating the past FTU RT acquisition system i.e. data are acquired at 500 kHz and then appropriately filtered and resampled via software at a sampling rate of 50 kHz in a window of 32 samples and the postprocessing sampling is 0.64

ms. The aim of this thesis is using in Real Time a SVD algorithm identifying

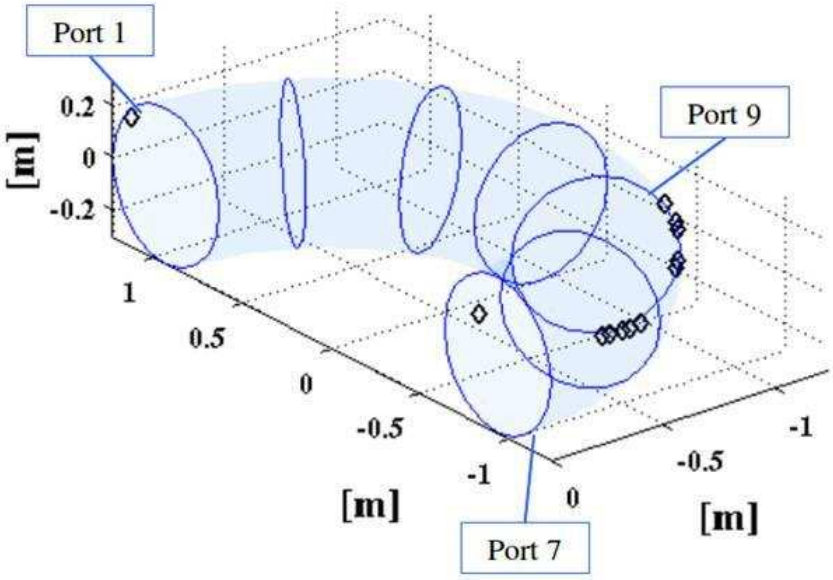

Figure 4.2: Configuration of the FTU Mirnov coils for the current work.

a warning signal for disruption. Before going into the details of the analysis we see the trend of the characteristic parameters introduced before, in order to distinguish a disruptive shot from a regular one. In the first chapter it was explained that a feature of disruptions is a typical current quench in the plasma current. In the third chapter have been introduced the quantities related to the presence of MHD instability, the entropy H

$$H = \frac{-\sum_{k=1}^{M} \frac{SV_k^2}{M} \log(\frac{SV_k^2}{M})}{\log(M)} \tag{4.1}$$

the P1 marker

$$P1 = \frac{SV_1^2 + SV_2^2}{\sum_{k=1}^{M} SV_i^2} \tag{4.2}$$

and we have explained that the entropy H describes the phase coherence in Mirnov coils, it is H is bounded between 0 and 1 and $H \to 0$ indicates more instabilities, P1 is related to the presence of the first mode and more $P1 \to 1$, more the first mode is unstable. In this chapter and in next one we explain the use and importance of these two indicators in the investigation of a real-time disruption precursor. We represent graphically the temporal trend of the current and the entropy for the two types of event: disruption and regular termination. In figure 4.3 is shown the different time evolution of plasma

current for a disruptive shot (red) and for a regular termination (green). The disruptive shot presents a current quench at the time t_{CQ}=1.20 s. In fig. 4.4 is shown the different trend of entropy for the same discharges. In the figure is in evidence the descending behavior of entropy for the disruptive shot at the disruption time. Since in the presence of a low value of entropy we expect more instabilities and consequently the probability of a disruptive event increases, then the first step in this analysis is to calculate the average value of entropy H in a time window of 10 ms around its minimum, $\langle H_{min} \rangle$. These quantities are shown for the whole dataset in figure 4.6.

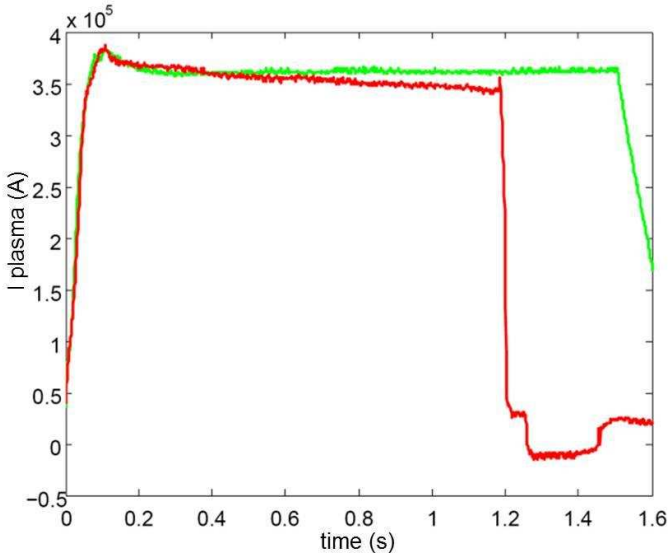

Figure 4.3: Plasma current trend for the disruptive shots 36239 (red) and for the regular termination 36245 (green).

A good estimator as disruption precursor will maximize the number of disruptions recognized (right alarms) and minimize the number of false alarms (regular shots exchanged for disruptions). The reference level of entropy detected depends on the specific characteristics of the sensors as position, noise and so on. The algorithm reads magnetic signals coming from 12 Mirnov coils and from the history reconstruction of the coils in FTU it is possible to distinguish six different configurations. In this work have been considered both an analysis of the entire database and the analysis for three different configurations. These three configurations are chosen such as those that contain a great number of experiments, sufficient for statistical analysis. Consider a particular configuration is equivalent to consider a limited period of time. The three different configuration are called 1, 3, 12.
In the set of disruptive shots the goal of this work is to maximize the num-

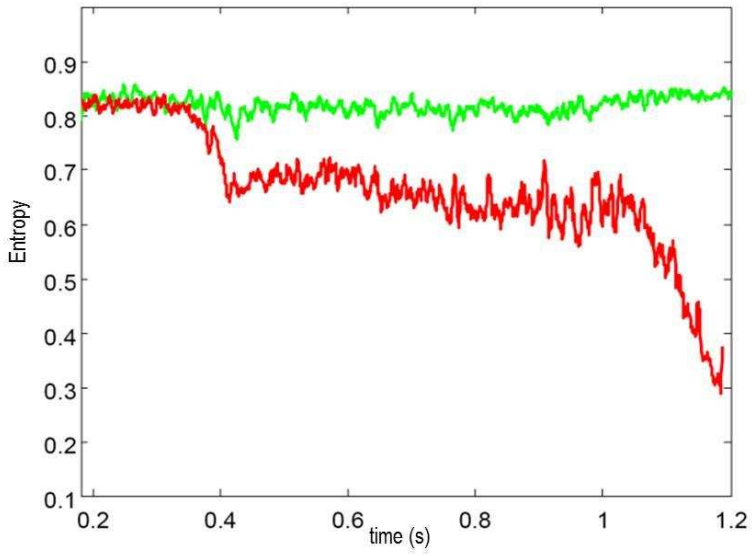

Figure 4.4: Entropy trend for the disruptive shots 36239 (red) and for the regular termination 36245 (green).

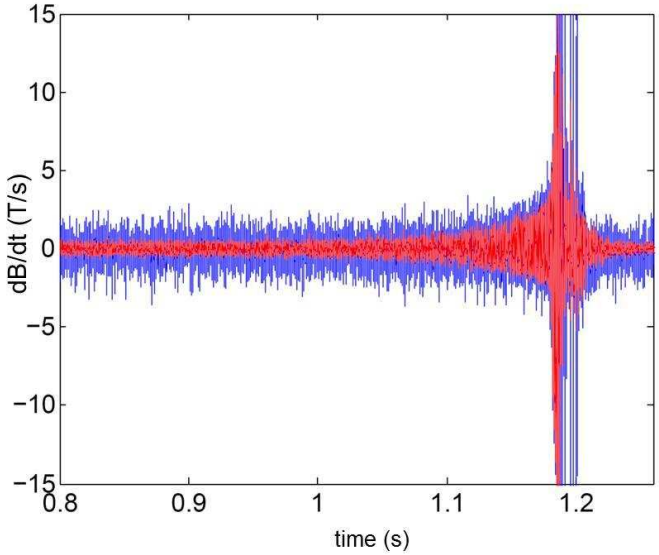

Figure 4.5: Exemple of fluctuation of poloidal magnetic field from a Mirnov coil signal for the disruptive shot 36239. The peak of the fluctuation appears in correspondence of t_{CQ}=1.20 s.

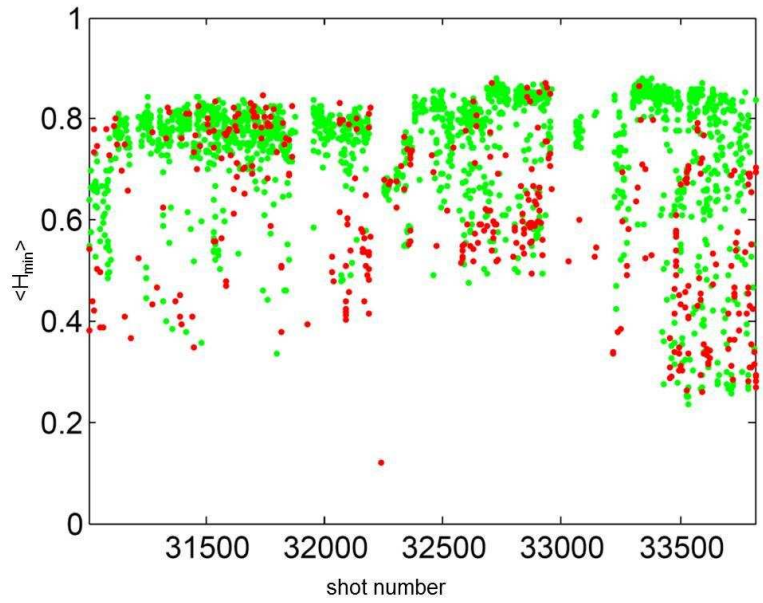

Figure 4.6: Entropy mean value for disruptive shots (red) and for regular terminations (green) for all shots. The mean value is calculated in a time window of 10 ms around the minimum.

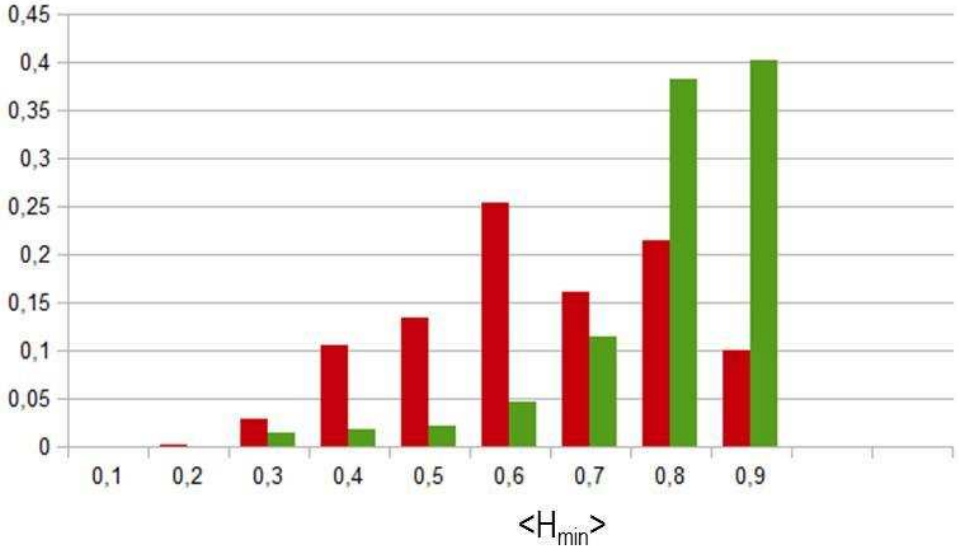

Figure 4.7: Percentage of disruptive shots (red) and regular terminations (green) for H intervals.

ber of right alarms and consequently minimize the number of missed alarms. Right alarms are disruptive shots recognized by the precursor signal as disruptions. In the ensemble of disruptive shots it is possible to identify the percentage of right alarm RA and missed alarms MA with the property $RA + MA = 100\%$.
In the set of regular terminations the goal of this work is to minimize the number of false alarms, these are the shots that do not have a disruptive current decay but the estimator recognizes as disruptive. In the ensemble of regular shots it is possible to identify the percentage of no alarms and false alarms with the property $NA + FA = 100\%$.
The two ensembles of events disruptive shots and regular termination are considered independent, they are shots selected and chosen from the database, their final behaviour is well known and the probability to recognize a disruptive event in the first set of events does not depend from the probability to recognize a regular termination in the second.
In order to determine a threshold that distinguishing the H value between disruptions and regular shots, we consider 10 entropy discrete intervals of step 0.1 with $0 < H < 1$ and we calculate the percentage of frequency of experimental date for each intervals as shown in 4.7. While in figure 4.6 the values $\langle H_{min} \rangle$ for the two ensembles disruptive shots and regular terminations are not well distinct, in figure 4.7 appears clearly that the value of the higher peak related to disruption shots is lower then the higher peak related to regular terminations.
We consider the cumulative functions of the two sets in order to determine a threshold S on $\langle H_{min} \rangle$. This threshold S should consent to individuate right alarm as disruptive events under the threshold S and no alarms as regular shot events over the threshold S. Let $f_d(\widetilde{H})$ be the cumulative function for the set of event of disruptive shot, that is the probability to have a value of $\widetilde{H}$ between 0 and S

$$f_d(\widetilde{H}) = P_d(0 < \widetilde{H} < S). \tag{4.3}$$

Let $f_r(\widetilde{H})$ be the cumulative function for the set of event of regular terminations, that is the probability to have a value of $\widetilde{H}$ between 0 and S

$$f_r(\widetilde{H}) = P_r(0 < \widetilde{H} < S) \tag{4.4}$$

so the probability to have a value of $\widetilde{H}$ between S and 1 is $(1 - f_r)$

$$(1 - f_r(\widetilde{H})) = P_r(S < \widetilde{H} < 1). \tag{4.5}$$

The probability that a disruptive event is below threshold S and a regular event is above threshold S is given by the product of the cumulative

$$F(\widetilde{H}) = f_d(\widetilde{H}) \cdot (1 - f_r(\widetilde{H})). \tag{4.6}$$

The highest value of F identifies the best estimate of the threshold.
The best threshold corresponds to the peak value of F that results to be

$S = 0.7$. The value S=0.7 allows to recognize the 69% of right alarms and 79% of no alarms.
In fig 4.8 are shown the cumulative function for disruptive events $f_d(\widetilde{H})$ (red), cumulative function for regular terminations $f_r(\widetilde{H})$ (green) and product $F(\widetilde{H}) = f_d(\widetilde{H}) \cdot (1 - f_r(\widetilde{H}))$ (cyano).

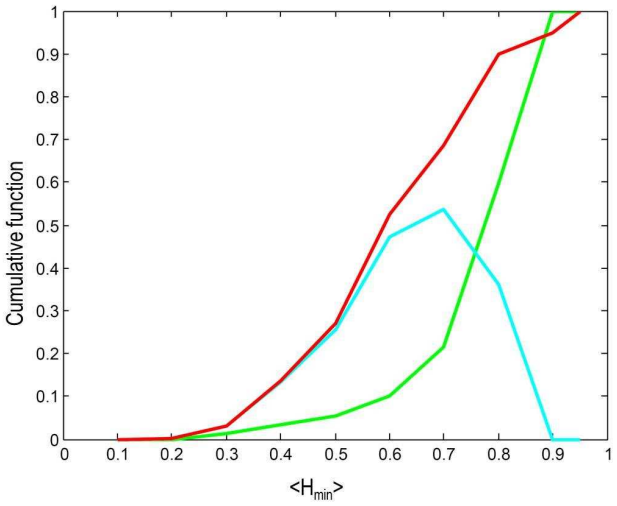

Figure 4.8: Cumulative function for disruptive events $f_d(\widetilde{H})$ (red), cumulative function for regular terminations $f_r(\widetilde{H})$ and product $F(\widetilde{H}) = f_d(\widetilde{H}) \cdot (1 - f_r(\widetilde{H}))$(cyano) .

The choice to evaluate H around the minimum is confirmed to be a good choice by the fact that for 60% of disruptive shots the difference between the time corresponding to the minimum of H and the time of disruption is less than 20 ms. The mean value of H around its minimum is relate to the probability of occurrence of a disruptive event but is not an estimator good enough for an efficient warning signal since the threshold found does not clearly separate the two sets of events, and it is needed a further investigation to determine a signal precursor more appropriate and efficient.

4.3 Study of entropy trend and time evolution of plasma discharge

At this point, the interest is to study in detail the time behaviour of entropy. At this stage, the attention is focused to a time interval of 300 ms. A time interval of 300 ms is sufficient both to appreciate the presence of instability that lead to disruption and take actions to mitigate it. This time interval for disruptive shots is taken before t_{CQ}, while for regular terminations we

considered 150 ms before H minimum and 150 ms after it.
This investigation reveals the existence of three different time behaviour: the time evolution of entropy before disruption can be descending, increasing or stationary while the entropy for a regular termination appears to be stationary. These different trends are well shown in 4.9 that represents entropy time evolution for the the disruptive descending and increasing plasma shots and 4.10 for stationary disruptive shot and for a regular termination.

We mentioned above the expression (see equation 4.2) and meaning of the marker P1, introduced in Chapter 3. In the previous chapter we have seen that an indicator of the presence of MHD activity is the marker P1. We want to analyse the simultaneous behavior of the two indicators of instability studying in detail the time evolution of plasma discharge in the plane H(t)-P1(t). For convenience of reading, we insert the graphics in a polar representation, in order to highlight the angular variation. The chromatic scale represents time axes, as illustrated in figure 4.13. The time evolution of plasma discharge in the plane H(t)-P1(t) for disruptive shots with the the same different trends descending, increasing and stationary is shown in figure 4.11. It is interesting to compare with the typical time evolution of plasma discharge in the plane H(t)-P1(t) for a regular termination, shown in figure 4.12.

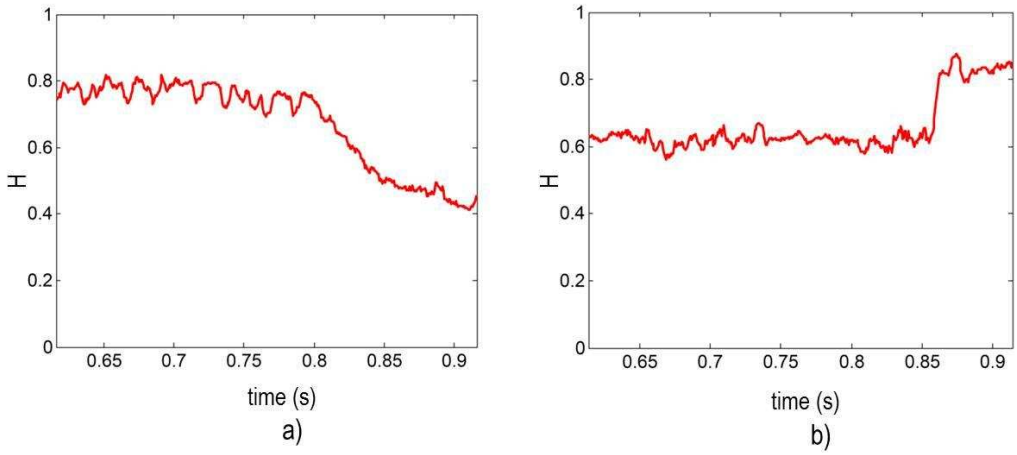

Figure 4.9: Entropy trend for a) disruptive descending shot 33337 and b) disruptive increasing shot 34393 in the time interval [t_{CQ}-300 ms, t_{CQ}].

Figures 4.9 and 4.10 underline entropy decreasing, increasing and stationary trend as time function, while in 4.11 and 4.12 it is possible to observe also that different plasma shots present a different angular variation. From this important evidence, therefore, has been analyzed in detail the time derivative of the ratio H/P1.

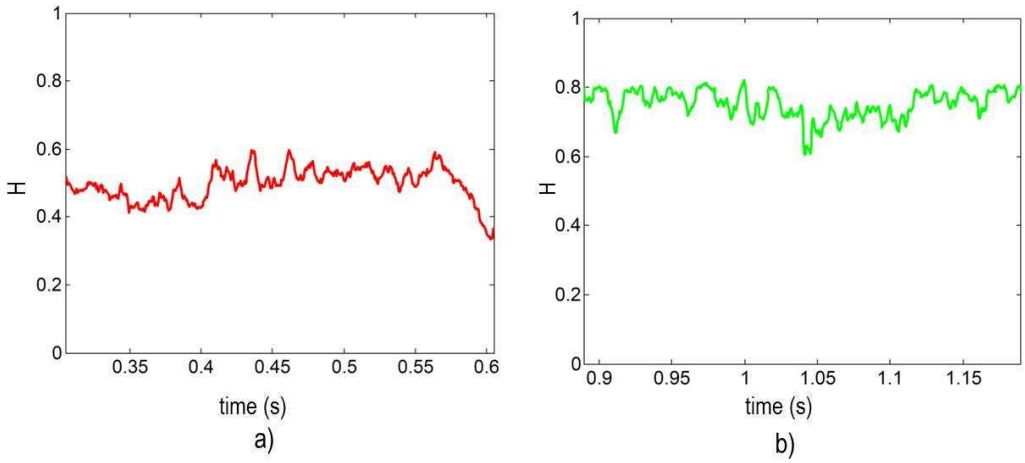

Figure 4.10: Entropy trend for a) disruptive stationary shot 31896 in the time interval [t_{CQ}-300 ms , t_{CQ}] and b) regular termination 33177 in the time interval [$t(H_{min})$-150 ms , $t(H_{min})$+150 ms].

4.4 Discriminator between disruptions and regular shots

The investigation exposed in the previous section has highlighted how the behavioral differences between a disruptive plasma shot and a regular termination can be distinguished not only by the value and time trend of entropy, but also from the simultaneous evaluation of entropy and P1 marker during plasma discharge.
One important step in this analysis is to explore the behavior of plasma discharge in the plane H(t)-P1(t). In order to find a disruption precursor we study the trend of H(t)-P1(t), of the time derivative of H(t)/P1(t) and of the square root of moving variance of the time derivative of H(t)/P1(t). In this section, we illustrate in detail the study of the square root of moving variance, *mvd*, which appears to be the best candidate as an indicator of disruption. Being

$$x(t) = \frac{d}{dt}(\frac{H}{P1}) \tag{4.7}$$

the moving variance mvd^2 is computed in time interval of 40 samples and is defined as the difference between the moving average of the x^2, $E[x^2(t), t]$ and the square of the moving average of x, $E[x(t), t]^2$

$$mvd^2 = E[x^2(t), t] - E[x(t), t]^2 \tag{4.8}$$

We show the temporal trend of the variable *mvd* to see if it allows to discriminate a disruptive event by a regular, which means if we can identify

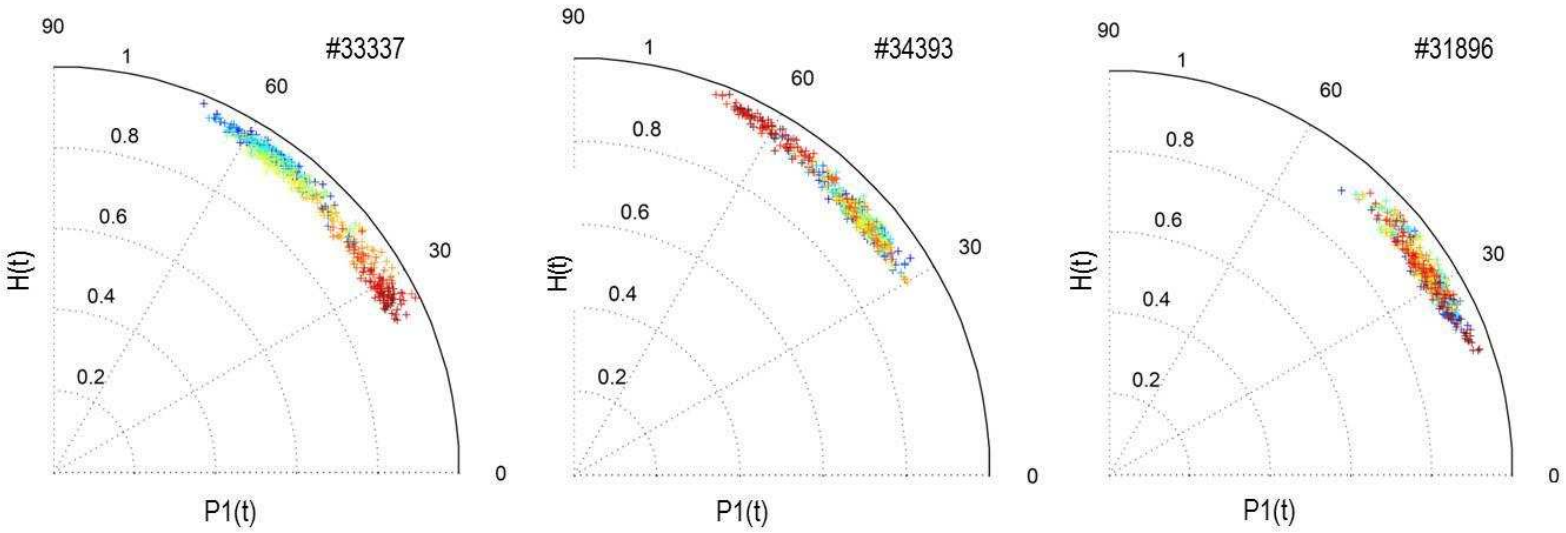

Figure 4.11: Time evolution of plasma discharge in the plane H(t)-P1(t) for descending shot 33337, increasing shot 34393 and stationary shot 31896 in the time interval [t_{CQ}-300 ms , t_{CQ}]. The meaning of chromatic scale is shown in figure 4.13.

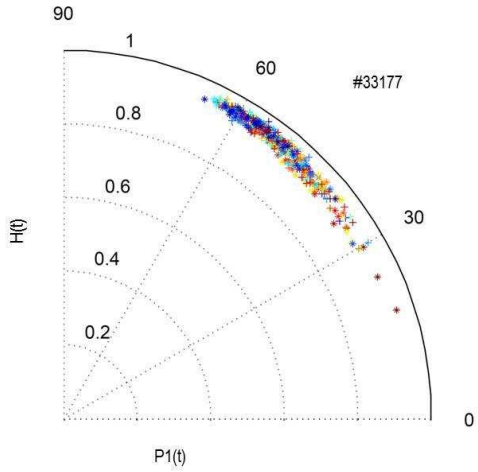

Figure 4.12: Time evolution of plasma discharge in the plane H(t)-P1(t) for regular termination 33177 in the time interval [$t(H_{min})$-150 ms , $t(H_{min})$+150 ms]. The meaning of chromatic scale is shown in figure 4.13.

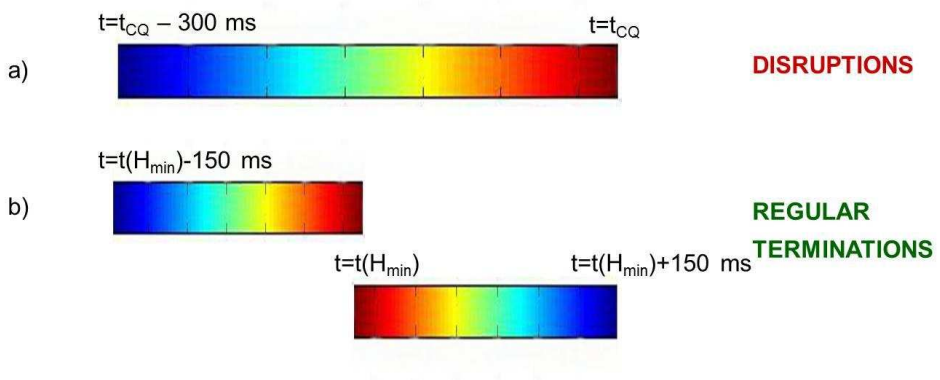

Figure 4.13: Chromatic Scale for a) disruption pictures 4.11 and b) regular termination 4.12.

in it a precursor of disruption. In figure 4.14 it is shown the comparison between the *mvd* trend for six different disruptive plasma shots (red) and the trend for 6 different regular termination (green) in configuration 3. The different behavior is clear so we try to identify a discriminator for disruption prediction on *mvd* and establish a threshold on it. From 4.14 we can

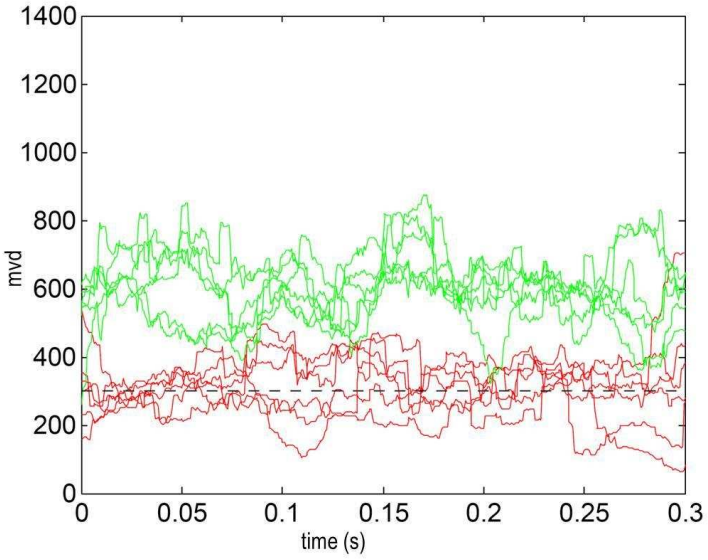

Figure 4.14: Comparison of the square root of the moving variance trend between six disruptive shots (red) and six regular termination (green) chosen in configuration 3. The dot line represent the best threshold ThMVD=300.

observe that disruptions appear to have lower values of *mvd* than regular terminations. We proceed with the statistical analysis in order to determine a threshold on *mvd* below which an event can be considered as disruption. We calculate for both the ensembles the percentage of shots that goes below the threshold ThMVD=50, 100, 150 ... 500 more than N=1,5,10,20 times in the discharge. Disruptive discharges that go below the threshold more than N times in the shot are recognized as right alarms RA otherwise as missed alarms MA. Regular terminations that never go below threshold more than N times in the shot are recognized as no alarms NA, otherwise as false alarms FA. The percentage of right alarms RA and no alarms NA as functions of the threshold are shown in 4.15 for configuration 3. The probability to recognize a right alarms in disruption ensemble and at the same time no alarms in regular termination ensemble as function of the threshold is the result of the product between right alarms and no alarms. The threshold corresponding to the peak of this product, shown in figure 4.16 individuates the best threshold that maximize the probability to have at the same time RA in the

first set and NA in the second one. From this analysis we can establish that a threshold ThMVD = 300 provide to recognize a right alarm if the *mvd* of a disruptive shot drops below the threshold for more than N=5 times.
This analysis has been done for the whole time duration of the shot neglecting the first 300 ms to avoid physics plasma transients. From the study of the time evolution of the plane H(t)-P1(t) we can conclude that the square root of the moving standard deviation of the time derivative of H/P1, *mvd* is a good discriminator between the two ensembles in order to determinate a threshold that allow to recognize disruptions. In table 4.2 are summarized all the results. In configuration 3, ThMVD=300 consents to recognize the 82% of right alarms and 77% of no alarms.

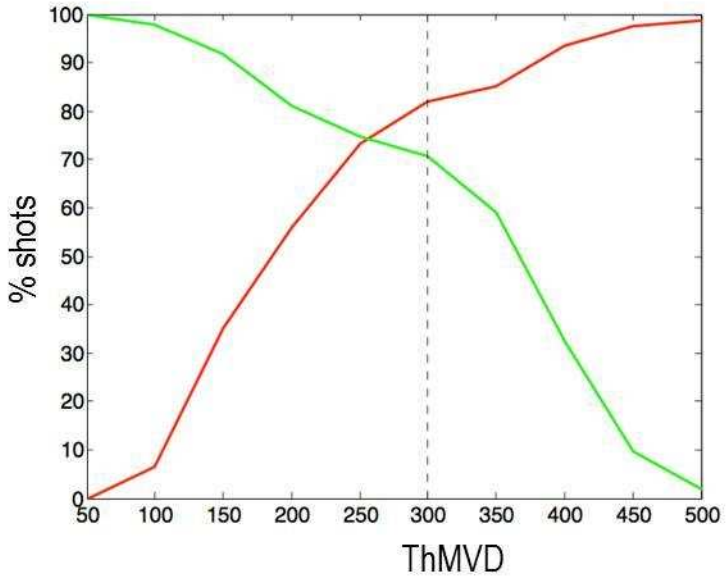

Figure 4.15: Percentage of Right Alarm RA (red) and No Alarm (green) as function of ThMVD for configuration 3. The dot line represents the threshold ThMVD=300.

4.5 Disruption alarm time

The efficacy of a good disruption precursor signal is not only related to the recognition of the higher number of right alarms and the lower number of false alarms, but also requires the detection of an alarm time sufficient to take precautionary measures. The concept of sufficient time depends on the avoidance and/or mitigation techniques that are used and on the inherent time scale of the tokamak. At FTU the avoidance and mitigations are real-

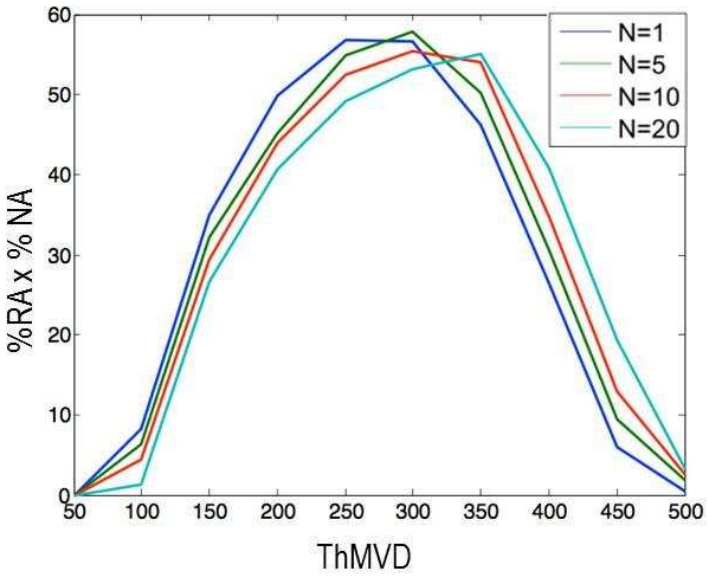

Figure 4.16: Product between percentage of Right Alarms RA and No Alarms NA as function of the threshold ThMVD for configuration 3. The high peak for N=5 is in correspondence of ThMVD=300.

Configuration	1	3	12	all
threshold value	300	300	150	250
RA	70%	82%	52%	67%
MA	30%	18%	48%	33%
NA	70%	71%	77%	73%
FA	30%	29%	23%	27%

Table 4.2: Summary of FTU results: percentage of right alarms (RA), missed alarms (MA), no alarms (NA) and false alarms (FA) individuated with a threshold on the square root of the moving variance of the time derivative of H/P1. The results are presented for every configurations and for all the data analized.

ized through injection of ECRH [21].
Let's see how to determine an alarm time on the precursor based on the average value of H around the minimum. The threshold has been established finding the absolute minimum value of H during the plasma discharge and considering an average value in a time window of 10 ms around the minimum. The result does not change by varying the time window: 10 ms, 20 ms and 40 ms give the same result. We have established that a shots in the ensemble of disruptive shots with $\langle H_{min} \rangle < 0.7$ will be recognized as a right alarm. Since this research will be implemented in a real-time algorithm it is useful to define an alarm time using the indicator $\langle H_{min} \rangle$ as precursor. The idea is to determine for every disruptive discharge after how many seconds the value of the entropy calculated by SVD falls below the threshold $S = 0.7$ at least 5 times. We neglect the first 300 ms to avoid plasma physics transients and being experimental data so fluctuating we consider a moving average of the entropy H. The numbers of disruptive shots recognized as right alarms at the time t_{ALARM} as function of the time distance $t_{CQ} - t_{ALARM}$ from the disruption are shown in figure 4.17. From the figure we can extract that varying $t_{CQ} - t_{ALARM}$ the 56% of disruptions are recognized 100 ms in advance, the 63% 50 ms in advance and the 69% 20 ms in advance.
The research of disruption alarm time for the precursor based on *mvd* completes the work. The alarm time is define as the time corresponding to have 5 points of *mvd* under the threshold 300. We take in consideration plasma disruptive shots of the period relative to configuration 3 where the disruption precursor is able to recognize up to 82% of the disruptions. Neglecting the first 300 ms to avoid plasma physics transients, the results of the computation of the warning time are shown in figure 4.18 In this way for configuration 3, with a threshold on mvd=300 the 79% of disruptions are recognized with 20 ms of warning time before the plasma current quench, the 74% 50 ms in advance and the 62% 100 ms in advance. The results are summarized in table 4.3.

warning	% RA H<0.7	% RA mvd<300
$t_{CQ} - t_{ALARM} > 20ms$	69%	79%
$t_{CQ} - t_{ALARM} > 50ms$	63%	74%
$t_{CQ} - t_{ALARM} > 100ms$	56%	62%
t_{CQ}	69%	82%

Table 4.3: Summary of FTU results: percentage of right alarms in relation to the warning time for both the indicators.

The algorithm based on the SVD analysis of the MHD activity signals from a set of FTU Mirnov coils provide a disruption precursor able to recognize up to 82% of the disruptions, and 79% of disruptions are recognized with

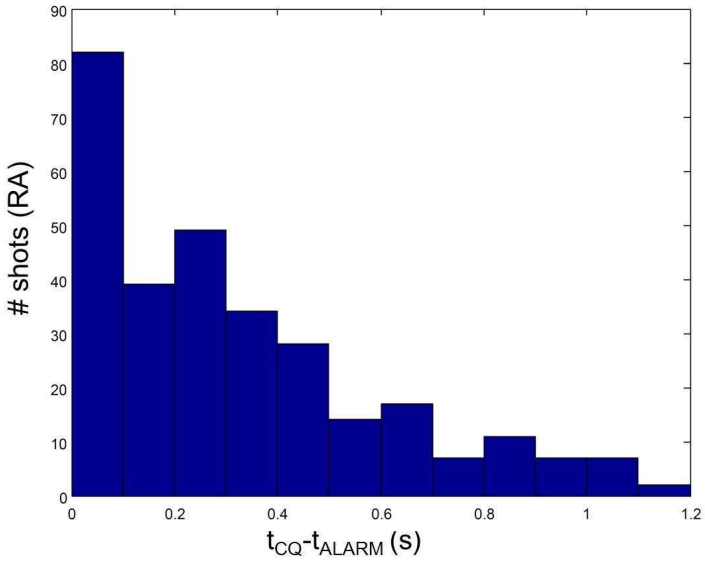

Figure 4.17: Number of right alarms recognised with the indicator $\langle H_{min} \rangle$ in the time interval $t_{CQ} - t_{ALARM}$. The 69% of disruptions are recognized at least 20 ms from the disruption.

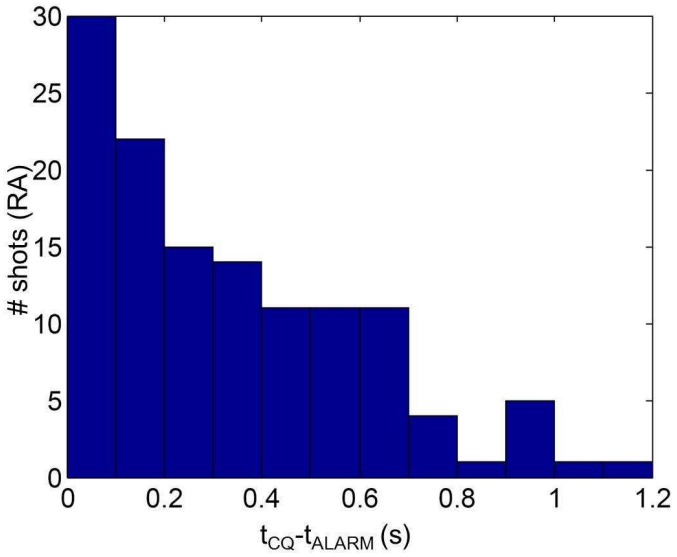

Figure 4.18: Number of right alarms recognized with the indicator *mvd* in the time interval $t_{CQ} - t_{ALARM}$ for configuration 3. The 79% of disruptions are recognized at least 20 ms from the disruption.

20 ms of warning time before the plasma current quench. In FTU tokamak, experience confirms that 20 ms are enough to trigger actions for avoiding or mitigating current decay and disruption.

4.6 Results and conclusions

The physical investigation of a precursor signal of disruption and the identification of a sufficient alarm time to take measures of action, suggests the possibility to refine and implement a real-time algorithm for disruption predictions, based on the SVD analysis of the MHD activity signals from a set of FTU Mirnov coils. Since this method appears to be efficient for the FTU tokamak, the same analysis has been developed and applied to the JET tokamak, as explained in the next chapter.
This work has been included in the poster "Real-time analysis of magnetohydrodynamics instabilities in the FTU tokamak" presented at the Conference "Italian National Conference on Condensed Matter Physics", FisMat 2013, Politecnico di Milano, Milan (Italy), 09-13 September 2013 [39].

Chapter 5

JET Data Analysis

In the previous chapter has been shown the research of a disruption precursor through the development of algorithms based on the SVD analysis of signals from Mirnov coils for FTU. The results appear to be interesting and encouraging, the robustness of the method can be demonstrated, for example, testing the analysis on the experimental data of another machine. In this chapter the analysis already carried on FTU is repeated on JET, a machine very different for the shape, the size, the characteristic parameters and the plasma confinement. Being JET a device more complex, in which can occur further physical phenomena, it is interesting to see if the same method is efficient. Moreover, since bigger is the tokamak more the consequences of disruption are dangerous, in a big size device as JET the research of a disruption precursor is very important.

5.1 JET Joint European Torus

JET Joint European Torus is one of the world's largest tokamaks, with a plasma volume of about 90 m^3 and it was built up at the begin of 80s in Culham Science Centre (Oxfordshire, UK). It is a D-shape plasma tokamak with the major radius of 2.96 m, the minor horizontal radius of 0.96 m and the vertical minor radius of 1.60 m. It is the only machine capable of operating with the deuterium-tritium fuel mix of future commercial reactors. In 1997 a world record was achieved at JET: 16 MW of fusion power were produced from a total input power of 24 MW, a 65% ratio, the equivalent to a release of 22 MJ of energy. Today, its primary task is to prepare for the construction and operation of ITER, acting as a test based for ITER technologies and plasma operating scenarios [1]. The major innovation and characteristic of JET is the D-shape toroidal field coils and the D-shape plasma cross section with an elongation of 1.7.
The main parameters of JET device [40] are summarized in table 5.1 and a schematic representation is shown in figure 5.1.

Parameters	value
Major radius (m)	2.96
Horiz. minor radius (m)	0.96
Vert. minor radius (m)	1.60
Toroidal B field (T)	3.5–4
Plasma current (MA)	4.8
Max flat top duration (s)	60
Maximum central density (m^{-3})	$2\text{x}10^{20}$
Maximum electron temperature (keV)	20

Table 5.1: Main physical parameters of Joint European Torus.

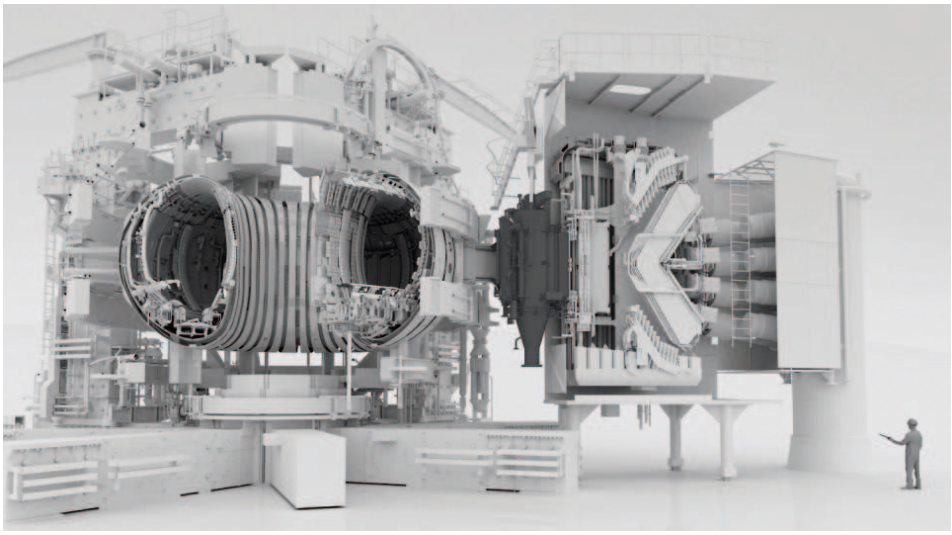

Figure 5.1: Simplified cutway design of JET machine. The person on the bottom gives an idea of the dimensions [1].

5.2 JET data analysis

The shots selected for the analysis are chosen from JET database between 2012-2013. For this time period the configuration of 16 Mirnov coils is known. We selected 2044 plasma shots, 457 disruptive shots and 1587 regular terminations. Before starting the analysis it was necessary to develop an algorithm in MATLAB to verify the presence of Current Quench and computed the current quench time t_{CQ}. The algorithm for Current Quench detection

implemented is similar to the one used at FTU. For disruptive shots, the disruption time is define as the plasma current quench time t_{CQ}. This parameter is computed by the comparison with the measured plasma current and reference current and by means of moving average of plasma current derivative $\frac{dI_p}{dt}$. If $\frac{dI_p}{dt}$ exceeds a suitable threshold at time t_{CQ} disruption event is recognized. Reference current is defined as the current that is expected to use in every single plasma experiment. Differently from FTU, this quantity is not a pre programmed current but it is constantly update in real time. From the comparison between plasma current and reference plasma current has been possible to select a stationary current interval in order to choose regular shots.
The time length of typical JET plasma shots is about 60-70 seconds, the current ramp during 20 seconds. It is not possible to test the algorithm for the whole plasma discharge duration and we computed the analysis for just 1 second. Even here all the codes are written in MATLAB, in particular the call to the reading of the coils makes the code quite slow. An analysis in a time interval of 1 second remains sufficient for mitigation or take measures to avoid disruption.
For the 457 disruptive shots the selection of the time range for the analysis is trivial, 1 second before disruption. For the 1587 regular terminations we decided to consider a random time interval in a phase in which the current is stationary and are obviously available data of the coils which are not collected for all the duration of the discharge. In the selected shots, the absolute value of plasma current plateau has a mean value greater than 1 MA. The Mirnov signals are collected by the KC1M diagnostic system, a 2 MHz, 14 bits ADC system located at JET, it can be connected up to 23 magnetic signals from Mirnov coils and up to 32 non magnetic sources, as ECE. The analog signals from Mirnov coils are acquired at frequencies higher than those of interest for MHD activity, they are filtered and resampled and called by an appropriate routine at 250 kHz in the JET software, filtered first by a second order low pass butterworth filter at 60kHz after by a second order high pass butterworth and processed by SVD in windows of 256 samples and then postprocessed at 1 ms. In this analysis have been used 16 signals from Mirnov coils system, the typical configuration of the coils used in this work is shown in figure 5.2.

After the selection of disruptive shots with the calculation of the corresponding current quench time, after the selection of regular terminations and the development of a code to determine the time range for the analysis, we follow the same procedure used at FTU. The analysis stars from the results of SVD, using the evident markers for the presence of instabilities, i.e. the entropy and P1 marker, in order to identify a threshold on the mean value of the entropy around its minimum and to verify if disruption precursor based on the square root of the moving variance of the time derivative of H/P1 is

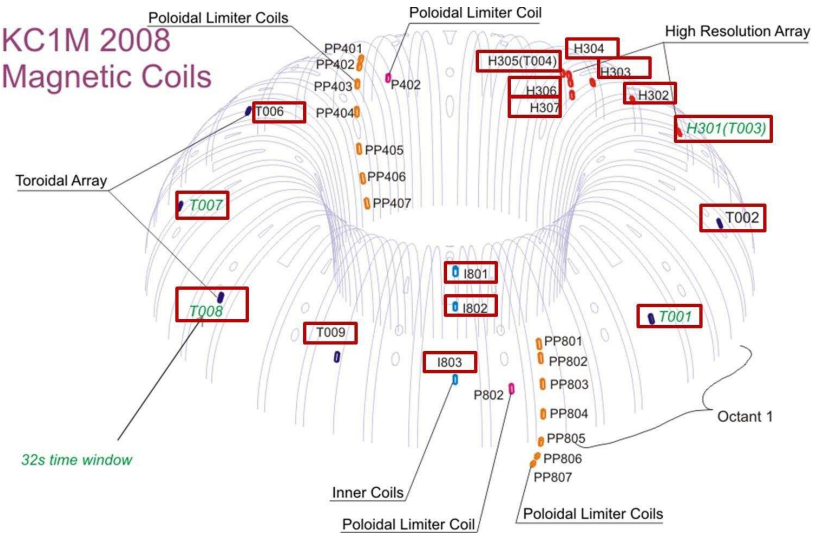

Figure 5.2: Configuration of the JET Mirnov coils [7]. The coils used in the current work are marked in red.

efficient.
Firstly it is helpful to see the different trends of the characteristic quantities for a regular termination and a disruptive shot. Figure 5.3 shows the comparison of plasma current between a regular termination 82036 (green) and a disruptive shot 82034 (red). As said above, the current plateau is longer then 20 s, to appreciate the difference and the current quench shape the figure is restricted before the disruption of the shots 82034 that occurs $t_{CQ} = 57.57$ s. In figure 5.4 we find the behaviour of the entropy, the indicator of our interest in order to predict disruption. We see the different trend between the regular shot 82036 and the disruptive shot 82034. This value, as said before, is calculated in just on second. The x axes represents the time, for the disruptive shot is the interval long 1 s before $t_{CQ} = 57.57$ s while for the regular termination is a random second in the flat top. Also in JET plasma discharges is evident a different behaviour of entropy trend for disruptive shots and regular terminations. We remember that in chapter 3 was pointed out that $H \to 0$ is index of the presence of instabilities and following the same steps of chapter 4 we comparison the average value of entropy H in a time window of 50 ms around its minimum, $\langle H_{min} \rangle$. The interval of 50 ms for the average has been chosen in relation to a postprocessing sampling less fine. The values of $\langle H_{min} \rangle$ for disruptive shots and regular terminations are shown for the whole dataset in figure 5.5.

The purpose of this analysis is to verify that the marker found maximizes the number of right alarm and minimize the number of false alarms. Also in

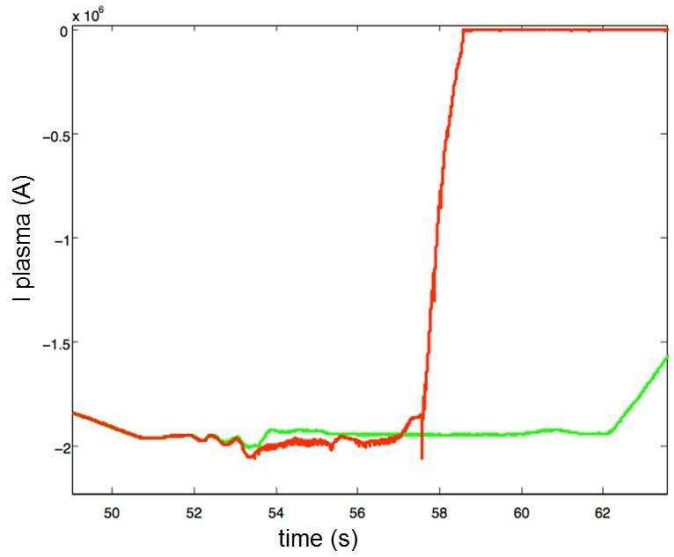

Figure 5.3: Plasma current trend for the disruptive shots 82034 (red) and for the regular termination 82036 (green).

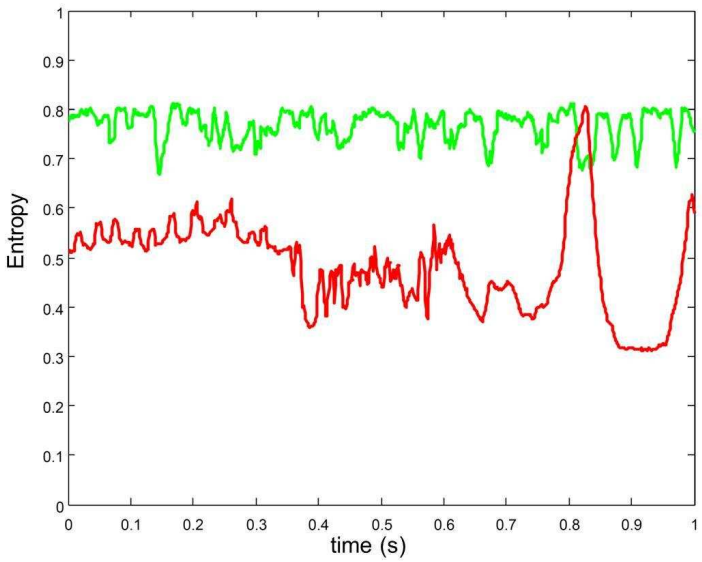

Figure 5.4: Entropy trend for the disruptive shots 82034 (red) and for the regular termination 82036 (green). The x axes represent the time, on [t_{CQ}-1s, t_{CQ}] for the disruptive shot, while the time for the regular termination is chosen random as explained in the text.

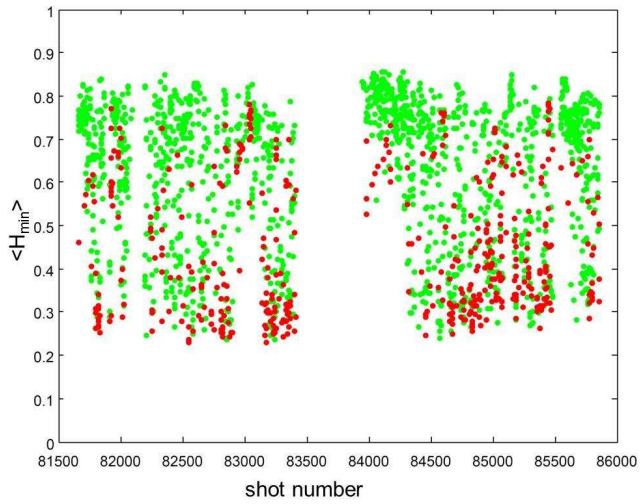

Figure 5.5: Entropy mean value for disruptive shots (red) and for regular terminations (green) for all shots. The mean value is calculated in a time window of 50 ms around the minimum.

this study the two ensembles of events disruptive shots and regular termination are considered independent.
In order to determine a threshold that distinguishing the H value between disruptions and regular shots, we consider 10 entropy discrete intervals of step 0.1 with $0 < H < 1$ and we calculate the percentage of frequency of experimental data for each intervals as shown in 5.6. We consider the cumulative functions of the two sets in order to determine a threshold S on $\langle H_{min} \rangle$. This threshold S should consent to individuate Right Alarm as disruptive events under the threshold S and No Alarms as regular shot events over the threshold S. Let $f_d(\widetilde{H})$ be the cumulative function for the set of event of disruptive shot, that is the probability to have a value of $\widetilde{H}$ between 0 and S

$$f_d(\widetilde{H}) = P_d(0 < \widetilde{H} < S). \tag{5.1}$$

Let $f_r(\widetilde{H})$ be the cumulative function for the set of event of regular terminations, that is the probability to have a value of $\widetilde{H}$ between 0 and S

$$f_r(\widetilde{H}) = P_r(0 < \widetilde{H} < S) \tag{5.2}$$

so the probability to have a value of $\widetilde{H}$ between S and 1 is $(1 - f_r)$

$$(1 - f_r(\widetilde{H})) = P_r(S < \widetilde{H} < 1). \tag{5.3}$$

The probability that a disruptive event is below threshold S and a regular event is above threshold S is given by the product of the cumulative

$$F(\widetilde{H}) = f_d(\widetilde{H}) \cdot (1 - f_r(\widetilde{H})). \tag{5.4}$$

The highest value of F identifies the best estimate of the threshold.
The best threshold corresponds to the peak value of F that results to be $S = 0.6$. The value S=0.6 allows to recognize the 79% of right alarms and 67% of no alarms.
In fig 5.7 is shown the cumulative function for disruptive events $f_d(\widetilde{H})$ (red), cumulative function for regular terminations $f_r(\widetilde{H})$ (green) and product $F(\widetilde{H}) = f_d(\widetilde{H}) \cdot (1 - f_r(\widetilde{H}))$ (cyano). We can conclude that the analysis carried out on FTU has also a positive result on JET. The indicator based on the average value of entropy around its minimum has been confirmed to be related to the probability of disruption and appears to be a good discriminator between the two sets disruptions-regular terminations.

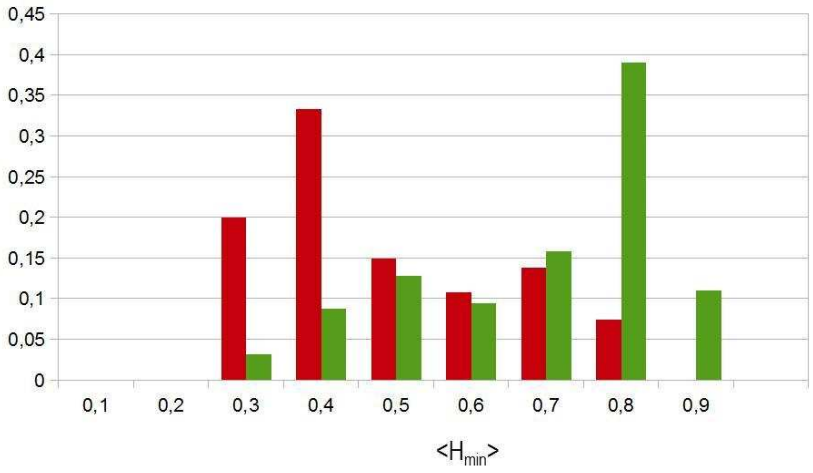

Figure 5.6: Percentage of disruptive shots (red) and regular terminations (green) for H intervals.

5.3 Study of entropy trend and time evolution of plasma discharge

We analyse here the entropy trend behaviour limiting the analysis in a time window of 300 ms, i.e. the interval [t_{CQ}-300 ms , t_{CQ}] for disruptive shots and time interval [$t(H_{min})$-150 ms , $t(H_{min})$+150 ms] for regular terminations. We recognize the presence of three different trend for disruptive shots ascending and descending shown in figure 5.8 and stationary that is compared to the entropy trend for a regular shots in figure 5.9.
We proceed with the investigation studying the simultaneous behavior of the

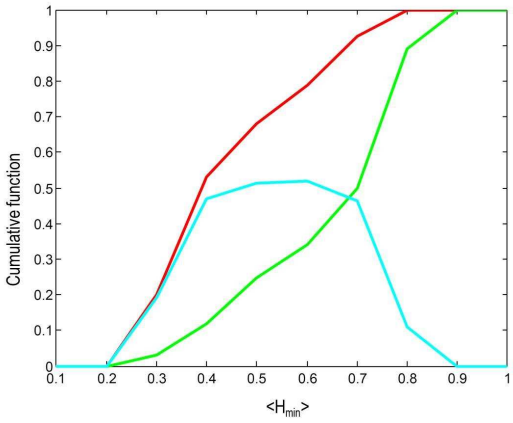

Figure 5.7: Cumulative function for disruptive events f_1 (red), cumulative function for regular terminations f_2 (green) and product $f_1 \cdot (1 - f_2)$ (cyano).

two indicators of instability studying in detail the time evolution of plasma discharge in the plane H(t)-P1(t). We find again the same three different behaviour ascending, descending and stationary for disruptive plasma shots that are shown in a polar representation for the time interval t_{CQ}-300 ms, t_{CQ} figure 5.10 while the chromatic scale is explained in figure 5.12. The comparison with the typical trend of a regular termination is shown in figure 5.11 in the time interval [$t(H_{min})$-150 ms , $t(H_{min})$+150 ms]. The polar representation allows to highlight the angular variation.

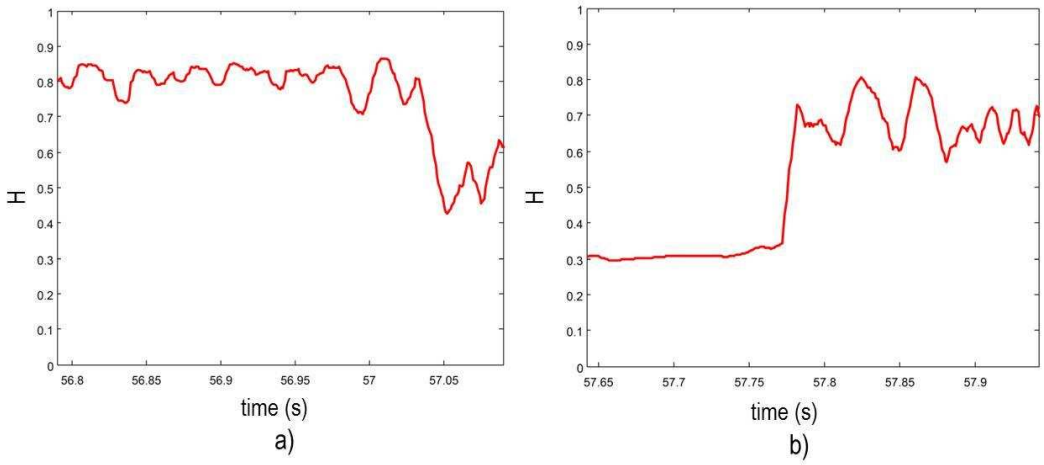

Figure 5.8: Entropy trend for a) disruptive descending shot 83980 and b) disruptive increasing shot 83187 in the time interval [t_{CQ}-300 ms , t_{CQ}].

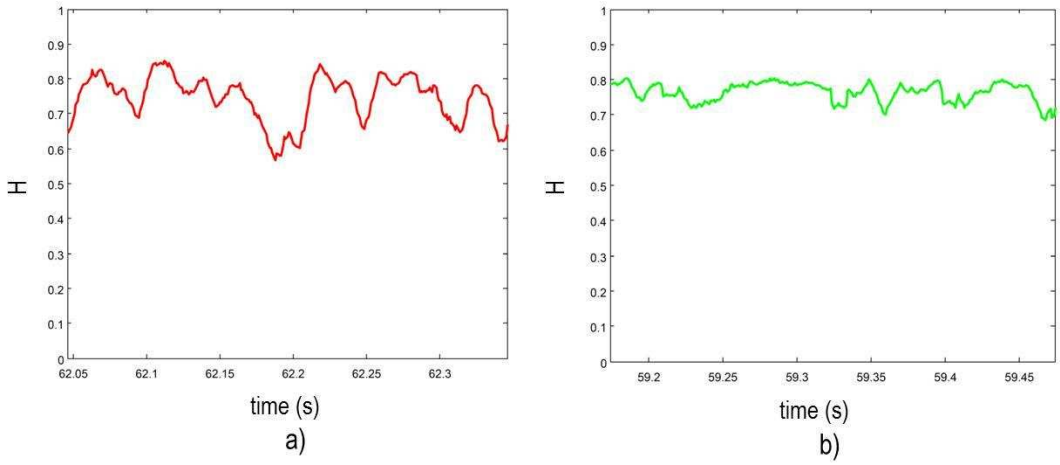

Figure 5.9: Entropy trend for a) disruptive stationary shot 84077 in the time interval [t_{CQ}-300 ms , t_{CQ}] and b) regular termination 82036 in the time interval [$t(H_{min})$-150 ms , $t(H_{min})$+150 ms].

5.4 Discriminator between disruptions and regular shots

The investigation exposed in the previous section confirmed the same behavioural differences between a disruptive plasma shot and a regular termination found for the analysis of FTU. Disruptive shots can be distinguished from regulars by the entropy and by the simultaneous time behaviour of entropy and P1 marker during plasma discharge. After these confirmations, we proceed computing the square root of moving variance of the time derivative of H/P1 in time windows of 40 samples, *mvd*. We show the temporal trend of this variable to see if it allows to discriminate a disruptive event by a regular, which means if we can identify in it a precursor of disruption. In fig 5.13 we represents the comparison of *mvd* for six different regular shots and six different disruptive shots. In order to determine a threshold on *mvd* below which an event can be considered as disruption we calculate for both the ensembles the percentage of shots that goes below the threshold ThMVD=20, 40, 60 ... 400 more than N=1,5,10,20 times in the discharge. Disruptive discharges that go below the threshold more than N times in the shot are recognized as right alarms RA otherwise as missed alarms MA. Regular terminations that never go below threshold more than N times in the shot are recognized as no alarms NA, otherwise as false alarms FA. The percentage of right alarms RA and no alarms NA as functions of the threshold are shown in 5.14.
The probability to recognize a right alarms in disruption ensemble and at

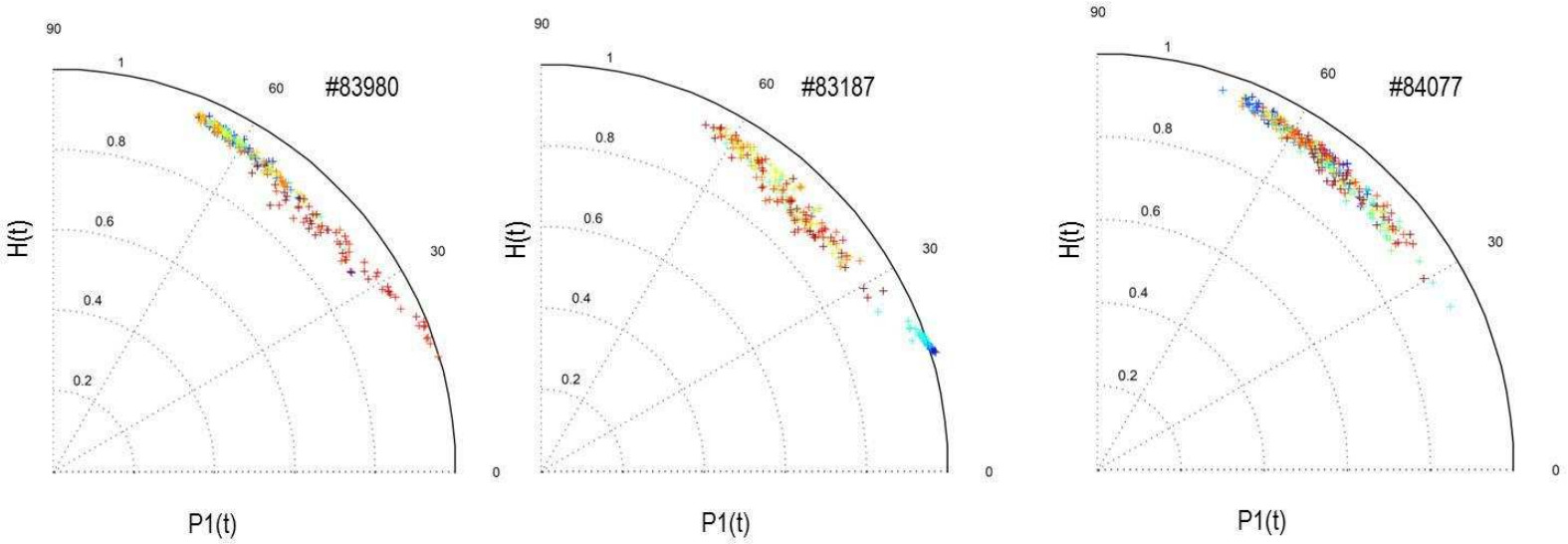

Figure 5.10: Time evolution of plasma discharge in the plane H(t)-P1(t) for descending shot 83980, increasing shot 83187 and stationary shot 84077 in the time interval [t_{CQ}-300 ms , t_{CQ}]. The meaning of chromatic scale is shown in figure 5.12.

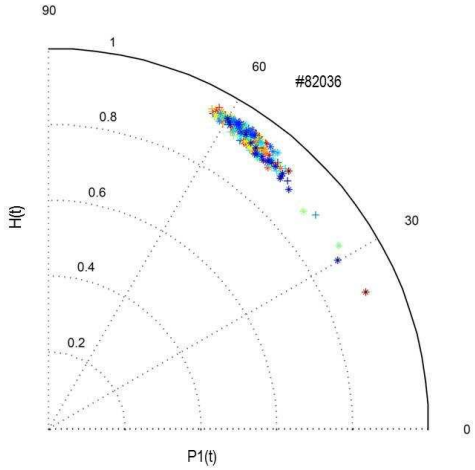

Figure 5.11: Time evolution of plasma discharge in the plane H(t)-P1(t) for regular termination 82036 in the time interval [$t(H_{min})$-150 ms , $t(H_{min})$+150 ms]. The meaning of chromatic scale is shown in figure 5.12.

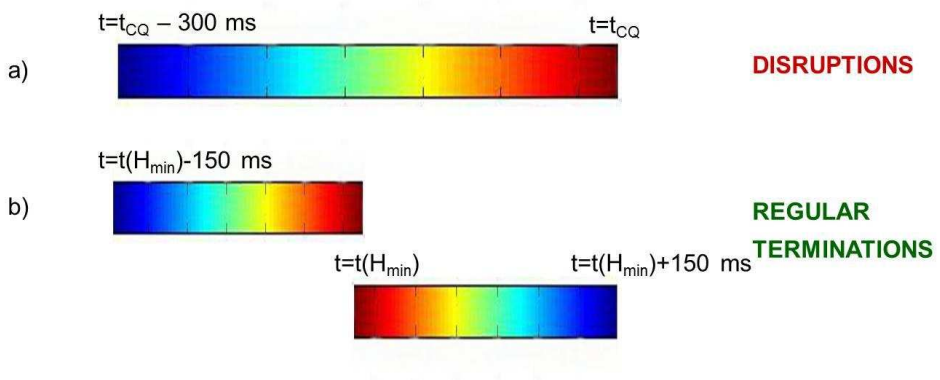

Figure 5.12: Chromatic Scale for a) disruption pictures 5.10 and b) regular termination 5.11.

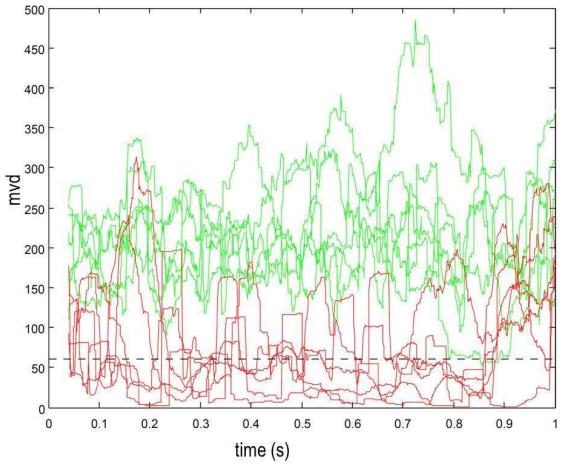

Figure 5.13: Comparison of square root of the moving variance trend between six disruptive shots (red) and six regular termination (green). The dot line represent the best threshold ThMVD found.

the same time no alarms in regular termination ensemble as function of the threshold is the result of the product between right alarms and no alarms. The threshold corresponding to the peak of this product, shown in figure 5.15 individuates the best threshold that maximize the probability to have at the same time RA in the first set and NA in the second one. From this analysis we can establish that a threshold ThMVD = 60 provides to recognize a right alarm if the *mvd* of a disruptive shot drops below the threshold for more than N times. Note from figure the that the threshold does not change varying N=1,5,10,20. We have verified that the detection rates are not significantly different varying N=1,5,10,20 and then we reasonably decide to fix N = 5, since we want to identify a disruptive event as soon as possible.
This analysis has been done in the whole time interval of 1 second where we calculate the quantities of interest for this analysis. From the study of the time evolution of the plane H(t)-P1(t) we can conclude that the research threshold of the square root of the moving variance of the time derivative of H/P1 (mvd) is able to discriminate the two ensembles disruptions-regular shots, a threshold ThMVD=60 allows to recognize the 63% of right alarms and 79% of no alarms.

5.5 Disruption alarm time

We have explained in section 4.5 that a good precursor requires the detection of an alarm time sufficient to take precautionary measures. We have determined an alarm time on the precursor based on the average value of H around

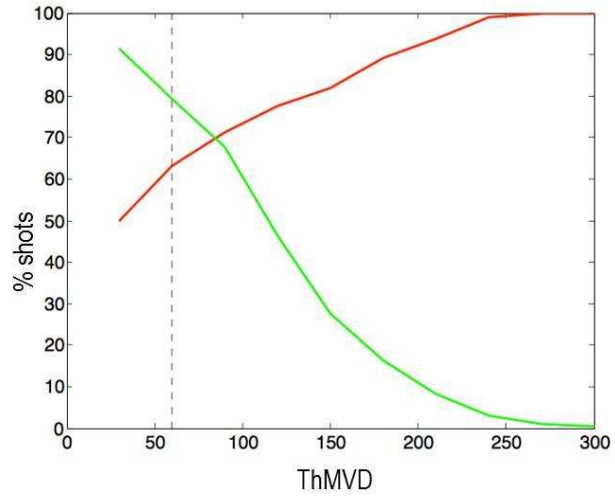

Figure 5.14: Percentage of Right Alarm RA (red) and No Alarm (green) as function of ThMVD. The dot line represent ThMVD=60.

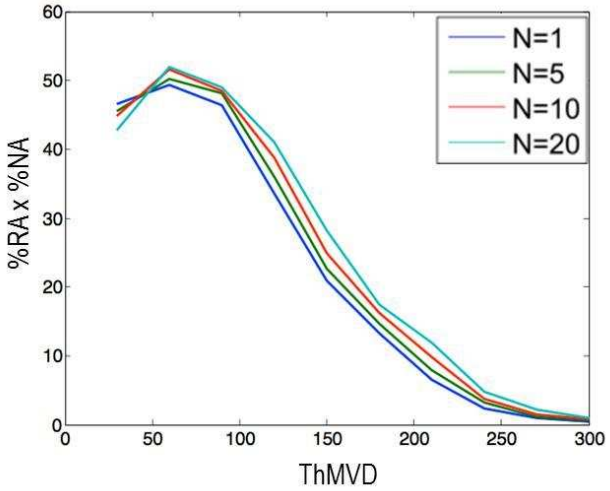

Figure 5.15: Product between percentage of Right Alarms RA and No Alarms NA as function of the threshold ThMVD. The high peak is in correspondence of ThMVD=60 and coincide for N=1,5,10,20.

the minimum. The threshold has been established finding the absolute minimum value of H during the plasma discharge and considering an average value in a time window of 50 ms around the minimum. We have established that a shots in the ensemble of disruptive shots with $\langle H_{min} \rangle < 0.6$ will be recognized as a right alarm. Since the aim of the research of a disruption detection is to implement it in a real-time algorithm it is useful to define an alarm time using the indicator $\langle H_{min} \rangle$ as precursor. We determine for every disruptive discharge after how many seconds the value of the entropy calculated by SVD falls below the threshold $S = 0.6$ at least 5 times. As explain at the begin of this chapter, the analysis has been carried out in just a second before the disruption. The experimental data are so fluctuating and we consider a moving average of the entropy H. The numbers of disruptive shots recognized as right alarms at the time t_{ALARM} as function of the time distance $t_{CQ} - t_{ALARM}$ from the disruption are shown in figure 5.16. From the figure we can extract that varying $t_{CQ} - t_{ALARM}$ the 72% of disruptions are recognized 500 ms in advance, 78% 100 ms in advance and the 79% 50 ms in advance. For a machine as JET 50 ms are enough to take precaution.

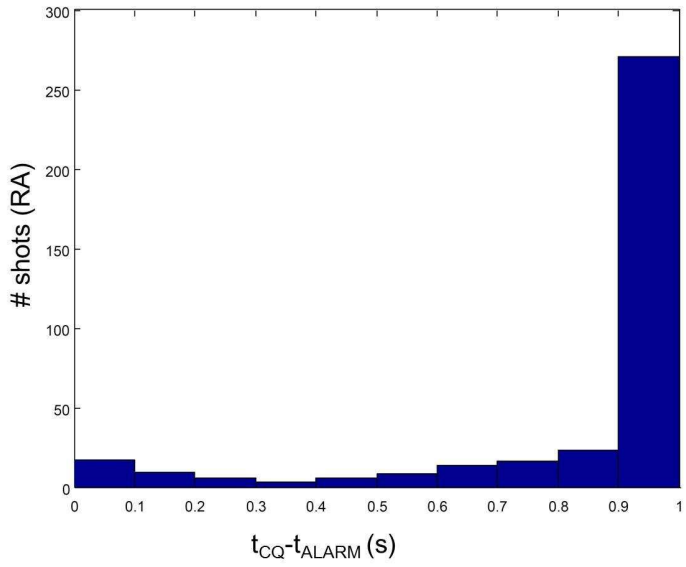

Figure 5.16: Number of right alarms recognised with the indicator $\langle H_{min} \rangle$ in the time interval $t_{CQ} - t_{ALARM}$. The 79% of disruptions are recognized at least 50 ms from current quench time.

The research of disruption alarm time for the precursor based on *mvd* completed the work. The alarm time is define as the time corresponding to have 5 points of *mvd* under the threshold 60. The numbers of disruptive

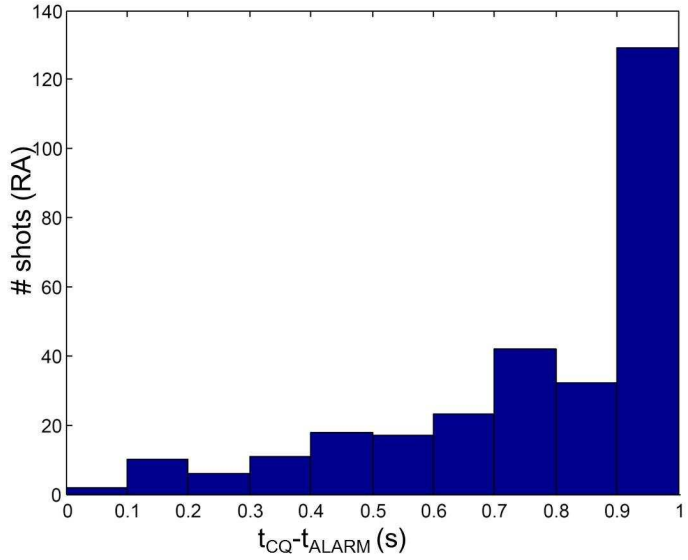

Figure 5.17: Number of right alarms recognized with the indicator *mvd* in the time interval $t_{CQ} - t_{ALARM}$. The 63% of disruptions are recognized at least 50 ms from the disruption.

shots recognized as right alarms at the time t_{ALARM} as function of the time distance $t_{CQ} - t_{ALARM}$ from the disruption is shown in figure 5.17 From the figure we can extract that varying $t_{CQ} - t_{ALARM}$ the 53% of disruptions are recognized 500 ms in advance, 63% 100 ms in advance and the 63% 50 ms in advance. For a machine as JET 50 ms are enough to take precaution.
All the results are summarized in table 5.2.

warning	% RA H<0.6	% RA mvd<60
$t_{CQ} - t_{ALARM} > 50ms$	79%	63%
$t_{CQ} - t_{ALARM} > 100ms$	78%	63%
$t_{CQ} - t_{ALARM} > 500ms$	72%	53%
t_{CQ}	79%	63%

Table 5.2: Summary of JET results: percentage of right alarms in relation to the warning time for both the indicators.

5.6 Results and conclusions

The analysis carried out for FTU for the research of a precursor disruption has been confirmed to be valid also for JET machine.

The development of set of algorithms based on the SVD analysis of the MHD activity signals from a set of JET Mirnov coils provide a disruption precursor based on the square root of the moving variance of the time derivative of H/P1 able to recognize up to 63% of the disruptions with 50 ms of warning time before the plasma current quench. For JET machine, an estimator based on the entropy mean value around minimum turns to be more efficient, being able to recognize up to 79% of the disruptions, with 50 ms of warning time before the plasma current quench.

Chapter 6

Conclusions

6.1 Summary

The aim of this work is the research of a disruption precursor and the development of a real time warning algorithm through the analysis of the results obtained by applying the Singular Value Decomposition (SVD) technique to Mirnov coils signals in plasma tokamaks.
While many techniques are available today for disruption avoidance and mitigation with some degree of successes, actually there is not any strategy that consent to fully predict and avoid all disruptions. The definition of a precursor signal of disruption is currently an interesting argument of research and in this PhD thesis an original method to determine a precursor signal is proposed.
SVD is a technique widely used in tokamaks for the study of MHD activity, it allows successfully to individuate the presence of the modes and to determine the mode numbers (n,m). The signals used in this analysis are fluctuations of the magnetic field caught by an array of small multiturn coils, the so called Mirnov coils. The signals have been opportunely filtered and resampled at the frequency of interest for MHD activity.
Through the Singular Value analysis is possible to extract useful markers of the instabilities presence, such as the Entropy H and the marker P1. The entropy H is proportional to the square of the normalized singular values and describes the phase coherence in Mirnov coils signals. The entropy can assume values in the range between 0 and 1 and lower values of the entropy H are indicative of the presence of instability in the plasma.
The P1 marker is the relative square magnitude of first couple of principal axes, it is bounded between 0 and 1. P1 is related to the presence of the first mode, i.e. the dominant couple (m,n). The more P1 is close to 1, the more unstable the first mode is. The presence of a mode indicates the growth of MHD activity, if the mode becomes unstable a disruption can occur.
2046 plasma discharges collected between 2008 and 2012 have been selected

from the FTU database. No threshold parametrization related to the plasma engineering parameters such as toroidal magnetic field, plasma current and density has been used. The signals considered have been normalized, having the advantage to be independent from sensor calibration and signal amplitude. We distinguished 1665 regular terminations and 381 disruptions without taking any classification on the causes that lead to a disruptive current quench.
From the application of SVD analysis to a set of FTU Mirnov coils [31] the entropy has been resulted to be a good marker for the presence of MHD instabilities. The investigation of the disruption precursor starts with the study of entropy time evolution during the plasma discharge. The two ensembles disruptive shots and regular terminations have been selected and considered separately, evaluating the mean value of entropy around its minimum. This is a good candidate in order to discriminate disruptive shots from regular terminations. The result of our analysis is the identification of a first precursor of disruption, based on entropy mean value around its minimum, able to recognize up to 69% of the disruptions with 20 ms of warning time before the plasma current quench. A further and deeper investigation of the plane H-P1 has brought to the individuation of a precursor based on the square root of the moving variance of the time derivative of the ratio H/P1. This last disruption precursor is able to recognize up to 82% of the disruptions, 79% at least 20 ms of warning time before the plasma current quench.
The same analysis have been adapted and repeated for Mirnov coils signals coming from JET machine, in order to test the robustness of the algorithm in different devices. We have analyzed 2044 plasma discharges collected between 2012 and 2013: 457 disruptive shots and 1587 regular terminations. Also in this case we do not distinguish disruption causes and no threshold parametrization has been established. The developed algorithms based on the SVD analysis of the MHD activity signals from a set of JET Mirnov coils provide a disruption precursor based on the square root of the moving variance of the time derivative of H/P1 able to recognize up to 63% of the disruptions, 50 ms before the plasma current quench. For JET machine, an estimator based on the entropy mean value around minimum seems to be more efficient, being able to recognize up to 79% of the disruptions, at least with 50 ms of warning time before the plasma current quench.

6.2 Future works

The results presented in this PhD thesis, based on the application of SVD algorithm in the research of a precursor signal of disruption are encouraging, but more detailed investigations are however needed. We show here the aspects that deserve to be explored and developed further to complete the

analysis.
We have pointed out that the analysis has carried out without any information about the engineering parameters of the machine. An interesting prosecution will be therefore try to parametrize the analysis contextualizing to physical meaning introducing for example thresholds related to plasma parameters such as magnetic field, plasma current and density.
The markers identified in this analysis can be used in order to classifying disruption causes. For this purpose it is mandatory: analyzing in detail the plasma discharge studying the evolution of different plasma and machine parameters, distinguishing not intentional from intentional disruptions and taking in account experimental conditions. Moreover, it should be important to focusing on the precursor phases preceding the instability and on the plasma development before the thermal quench. The investigation on a possible correlation between time dependence of the markers and the disruption evolution should be done for improve our analysis.

Bibliography

[1] www.efda.org.

[2] B. Esposito et al. Disruption Avoidance in the Frascati Tokamak Upgrade by Means of Magnetohydrodynamic Mode Stabilization Using Electron-Cyclotron-Resonance Heating. *Physical Review Letters*, 100, Feb 2008.

[3] J. Wesson. *The Science of JET*. 2000.

[4] J. Wesson. *Tokamaks*. Clarendon Press, Oxford, third edition, 2004.

[5] E. J. Strait et al. Chapter 2: Magnetic Diagnostics. *Fusion Science and Technology*, 53(2):304–334, Feb 2008.

[6] www.fusione.enea.it.

[7] S.N. Gerasimov. Status of the KC1M magnetic diagnostic. In *TFM meeting 24 March 2004*.

[8] J. D. Lawson. Some Criteria for Power Producing Thermonuclear Reactor. *Proc. Phys. Soc. B*, 70:6–10, 1957.

[9] I. Bandyopadhyay P. K. Kaw. The case for fusion. In *FUSION PHYSICS*, chapter 1, pages 17–20. INTERNATIONAL ATOMIC ENERGY AGENCY, Vienna, 2012.

[10] T. C. Hender et al. Chapter 3: MHD stability, operational limits and disruptions. *Nucl. Fusion*, 47(6):S128–S202, Jun 2007.

[11] G. Bateman. *MHD instabilities*. The MIT Press, 1978.

[12] J. A. Wesson et al. Disruptions in JET. *Nucl. Fusion*, 29(4):641–666, 1989.

[13] J. Hugill. Transport in tokamaks - a review of experiment. *Nucl. Fusion*, 23:331–373, 1983.

[14] P. C. de Vries et al. Survey of disruption causes at JET. *Nucl. Fusion*, 51:1–12, Apr 2011.

[15] P. C. de Vries et al. Influence of an ITER-like wall on disruption at JET. *Physics of Plasma*, 21:056101, 2014.

[16] G. Pautasso et al. Disruption causes in ASDEX Upgrade. In *41th EPS Conference on Plasma Physics*, 2014.

[17] Plasma Control ITER Physics Expert Group on Disruptions and ITER EDA MHD, ITER Physics Basis Editors. Chapter 3: MHD stability, operational limits and disruptions. *Nucl. Fusion*, 39(12):2251–2389, 1999.

[18] G.A. Ratta et al. An advanced disruption predictor for JET tested in a simulated real-time enviroment. *Nucl. Fusion*, 50:1–10, Jan 2010.

[19] J. M. Lopez et al. Implementation of the Disruption Predictor APODIS in JET Real Time Network using the MARTe Framework. In *Real Time Conference (RT)*. 18 th IEEE-NPSS, 2012.

[20] J. Vega et al. Result of the JET real-time disruption predictor in the ITER-like wall campaigns. *Fusion Engineering and Design*, 88:1228–1231, 2013.

[21] B. Esposito et al. Disruption control on FTU and ASDEX upgrade with ECRH. *Nucl. Fusion*, 49(6), May 2009.

[22] I. H. Hutchinson. *Principles of Plasma Diagnostics*. Cambridge University Press, second edition, 2002.

[23] S. V. Mirnov and I. G. Semenov. Investigation of the instabilities of the plasma string in the tokamak-3 system by means of a correlation method. *Sov. At. Energy*, 30(1):22, 1971.

[24] M. Bornatici et al. Electron cyclotron emission and absorption in fusion plasmas. *Nucl. Fusion*, 23(9):1153, 1983.

[25] E. de la Luna and JET-EFDA contributors. Physics of ECE Temperature Measurement and Prospects for ITER. Varenna (Italy), Sep 2007.

[26] E. Alessi et al. Real Time ECE-MIRNOV cross-correlations by dual phase lock-in technique in FTU tokamak. In *40th EPS Conference on Plasma Physics*, 2013.

[27] L. C. Ingesson et al. Chapter 7: Tomography diagnostics: bolometry and soft-X-ray detection. *Fusion Science and Technology*, 53(2):528–576, Feb 2008.

[28] N. Aubry et al. Spatiotamporal Analysis of Complex Signals: Theory and Applications. *Journal of Statistical Physics*, 64:683–739, 1991.

[29] C. Nardone. Multichannel fluctuation data analysis by the singular value decomposition method. *Plasma Physics and Controlled Fusion*, 34(9):1447–1465, Apr 1992.

[30] T. Dudok de Wit et al. The biorthonormal decomposition as a tool for investigating fluctuations in plasmas. *Phys. Plasmas*, 1(10):3288–3300, Oct 1994.

[31] C. Galperti et al. Development of real-time MHD markers based on biorthogonal decomposition of Mirnov coils signal. To be published on Plasma Physics and Controlled Fusion.

[32] C. Marchetto et al. MHD Structure Analysis by Singular Value Decomposition as a Tool for ECRH RT-Control of Instabilities on FTU. In *AIP Conference Proceedings, 1187*, pages 519–522, 2009.

[33] C. Marchetto et al. Sensitivity Analysis of SVD algorithm for real time mode control on FTU. In *37th EPS Conference on Plasma Physics*, 2010.

[34] C. Marchetto et al. Application on SVD algorithm to a set of Real Time Mirnov coil signals in FTU tokamak. In *39th EPS Conference and 16th Congress on Plasma Physics*, 2012.

[35] O. Tudisco et al. Chapter 8: The diagnostic systems in the FTU. *Fusion Science and Technology*, 45(3):402–421, May 2004.

[36] C. Gormezano et al. Chapter 1: The FTU program. *Fusion Science and Technology*, 45(3):297–302, May 2004.

[37] C. Mazzotta et al. On the effect of Neon injection on density peaking in FTU plasmas. In *40th EPS Conference on Plasma Physics*, 2013.

[38] C. Cianfarani et al. MHD signals as disruption precursors in FTU. In *40th EPS Conference on Plasma Physics*, 2013.

[39] M. Mosconi et al. Real-time analysis of magnetohydrodynamics instabilities in the FTU tokamak. In *Italian National Conference on Condensed Matter Physics, FisMat 2013*, 2013.

[40] J. Jacquinot et al. Chapter 2: Mission and highlights of the JET joint undertaking: 1978-1999. *Fusion Science and Technology*, 53(4):866–890, May 2008.

Acknowledgements

At the end of writing my dissertation I would like to express my gratitude towards people that supported me and improved my knowledge during my PhD activities.
I would like to thank my family for having supported and encouraged my studies.
I would like to thank Davide for his patience, for the love and for the constant presence.
I would like to thank Alessandro Moro, Edoardo Alessi, Lorenzo Figini and Marco Rossi for the scientific support, the help and the understanding.
Special thanks go to Dario Del Sorbo and Dimitri Batani.
I would like to thank my brother Boris and the friends who were close to me, especially Elisa, Moira, Ocleto and Simona.
It has been interesting to meet and share this phd with students from all over the world, in particular thanks for their presence and friendship to Alberto, Houriyed and Nima.
Finally, I would like to thank my supervisors Carlo Sozzi and Gabriele D'Antona for giving me the opportunity to work on this research project, for following me and teaching me a lot.